2023-08-14

Groundwater Flow Across the Coyote Wash Fault and Cedar Mesa Anticline near St. Johns, Arizona

Stephanie Lynn Latour
Brigham Young University

Groundwater Flow Across the Coyote Wash Fault and Cedar Mesa Anticline near St. Johns, Arizona

Stephanie Lynn Latour

A thesis submitted to the faculty of
Brigham Young University
in partial fulfillment of the requirements for the degree of

Master of Science

Stephen Nelson, Chair
Norm Jones
John McBride

Department of Geological Sciences

Brigham Young University

ABSTRACT

Groundwater Flow Across the Coyote Wash Fault and
Cedar Mesa Anticline near St. Johns, Arizona

Stephanie Lynn Latour
Department of Geological Sciences, BYU
Master of Science

As the demand for water increases across the southwestern United States, the region's utilization of and dependence on water stored in groundwater aquifers has risen in kind. The Coconino Aquifer (C-aquifer) underlies much of the southwestern Colorado Plateau and is a primary source of groundwater in northeastern Arizona. One of the largest commercial users of water from the C-aquifer in Apache County, Arizona, is Springerville Generating Station, a coal-fired power plant owned and operated by Tucson Electric Power. The area surrounding the power plant, located between the cities of Springerville and St. Johns, Arizona (the Springerville-St. Johns area), is geologically complex: it contains the Cedar Mesa anticline, an underlying CO_2 reservoir, extensive travertine deposits, and several faults, including the Coyote Wash fault. The Coyote Wash fault and Cedar Mesa anticline play a significant role in the relationships between the St. Johns CO_2 gas field, groundwater flow, and the travertine deposits. Yet, the interaction between the structures and the effect they have on groundwater flow is poorly constrained.

By mapping the subsurface geology utilizing borehole records and by creating a groundwater model of the area, this study determined that the Cedar Mesa anticline acts as a partial horizontal barrier to groundwater flow, whereas the Coyote Wash fault does not act as such a barrier. Particle tracking for the model indicates that despite the reduced water volume in the aquifer after decades of groundwater extraction, flow still occurs across the hinge of the Cedar Mesa anticline, accelerated by active pumping wells located west of the anticline axis. The model indicates that prior to the activation of the pumping wells, outflow from the C-aquifer would have occurred with greater frequency to Lyman Lake and along the extent of the Little Colorado River located downstream from the lake. The study also identified a zone of high hydraulic conductivity located between the Cedar Mesa anticline and the Coyote Wash fault that continues west of the Coyote Wash fault and may align with the Buttes anticline. This model of groundwater flow conditions improves the understanding of the complex subsurface geology and groundwater flow dynamics in the area.

Keywords: groundwater, model, MODFLOW, GMS, fault, Arizona, St. Johns, flow, anticline, particle tracking, Coconino aquifer, C-aquifer, Little Colorado River, water, Lyman Lake

ACKNOWLEDGMENTS

For their assistance with my thesis research, I'd like to thank the following people and groups:

Norm Jones

Steve Nelson

John McBride

Kevin Ray

Jeff Hammond and Tucson Electric Power

Graduate and undergraduate assistants: Cheyenne Lake, Ben Barton, Ama Voigt

Janis Flemming and Montgomery and Associates

To my best friends, Claire Ashcraft and Brian Reitz. All the effusive thanks I have would never be sufficient to convey my gratitude for all the support you have given me over the past several years. I would not have been able, nor desired, to achieve this without you. Thank you, a million times over.

I'm also grateful for the amazing friends I made during my time in BYU's Geology Department. Getting to know them has been one of my favorite parts of this experience and I will always treasure the time we shared. Although the COVID-19 pandemic was a difficult time to work through, it was made bearable by the unparalleled kindness of the Ashcraft family, Jenny, Gary, Isabelle, Sophie, and Claire, who took me in as one of their own during the lockdown. I'm very lucky to have found such a wonderful Utah family. Finally, thank you to my parents, Terry and Leslie Latour, for their dedication to raise me to be curious, adventurous, and to always persevere in spite of difficulties.

TABLE OF CONTENTS

LIST OF FIGURES

LIST OF TABLES

1. INTRODUCTION

As the demand for water increases across the southwestern United States, the region's utilization of and dependence on water stored in groundwater aquifers has risen in kind. The Coconino Aquifer (C-aquifer) underlies much of the southwestern Colorado Plateau and is a primary source of groundwater in northeastern Arizona (Hart et al., 2002; Jones and Robinson, 2021). One of the largest commercial users of water from the C-aquifer in Apache County, Arizona, is Springerville Generating Station (SGS), a coal-fired power plant owned and operated by Tucson Electric Power (TEP) (Jones and Robinson, 2021). The area surrounding the power plant, located between the cities of Springerville and St. Johns, Arizona (the Springerville-St. Johns area) (Figure 1), is geologically complex: it contains the Cedar Mesa anticline, an underlying CO_2 reservoir, extensive travertine deposits, and several faults, including the Coyote Wash fault. The Coyote Wash fault and Cedar Mesa anticline play a significant role in the relationships between the St. Johns CO_2 gas field, groundwater flow, and the travertine deposits. Yet, the interaction between the structures and the effect they have on groundwater flow is poorly constrained. The purpose of this study is to better understand the subsurface geology and groundwater flow across the Coyote Wash fault and Cedar Mesa anticline near SGS.

1.1 Regional Setting

The Springerville-St. Johns area is located at the south edge of the Colorado Plateau (Sirrine, 1958), just north of the Basin and Range province in eastern Arizona, along the northeast-trending Jemez lineament (Embid, 2009). The Jemez lineament is a tectonically active zone approximately 50 kilometers (km) wide characterized by normal, strike-slip, and en echelon faults, along with late Pliocene to Pleistocene volcanic fields (Aldrich and Laughlin, 1984). The Springerville volcanic field, located west of Springerville and southwest of St. Johns, is considered to be part of the Jemez lineament. This basaltic volcanic field, which is one of the largest in the western United States, covers 3,000 square kilometers (km^2) with numerous cinder cones and large-volume lava flows (Crumpler et al., 1994). The field is bounded on the northeast by the Concho fault (Figure 1), which also serves as the southwest

boundary of a structural depression containing over 250 km^2 of travertine (Sirrine, 1958; Crumpler et al., 1994). The northeast boundary of this depression is the Coyote Wash fault, a deeply penetrating normal fault that extends through younger sedimentary rocks into the granitic basement (Crumpler et al., 1994; Arizona Department of Environmental Quality [ADEQ], 2016). Yet, in many places, the Coyote Wash fault is spatially and structurally poorly constrained due to limited surface exposure and the extensive development of drainages through its southern segment (Crumpler et al., 1994; Miocic et al., 2019).

The stratigraphy of the Springerville-St. Johns area is primarily composed of sedimentary rocks ranging from Quaternary to Pennsylvanian in age, though no Jurassic rock is preserved. A nonconformity separates these sedimentary rocks from the Precambrian granitic basement (Figure 2) (Akers, 1964; Rauzi, 1999). Groundwater is present locally in the Quaternary deposits; however, the primary aquifer (the Coconino aquifer or C-aquifer) is composed of highly fractured Kaibab Limestone and Coconino Sandstone units, and in some places, the upper portions of the Supai Formation (Akers, 1964; Hart et al., 2002; ADEQ, 2016). The Coconino Sandstone and Kaibab Limestone are connected hydraulically with their laterally equivalent units, the Glorieta Sandstone and San Andres Limestone. The lateral transitions between these units approximately coincide with the Salt River lineament extension, which runs through this project's study area (Plates 5 and 6 in Rauzi, 2009). However, this study follows the terminology of the available borehole data and the primary groundwater monitoring report for the area (Montgomery and Associates, 2019), which use the nomenclature "Coconino Sandstone" and "Kaibab Limestone."

In the Springerville-St. Johns area, the primary surface-water source is the Little Colorado River, which has lowered the water table by incising through deposits of the Springerville volcanic field and older strata (Embid, 2009). The Little Colorado River is generally perennial between Springerville and St. Johns, though the river is dammed between the two cities to form the reservoir Lyman Lake (Mann and Nemecek, 1983). Flow downstream from Lyman Dam depends both on releases from Lyman Lake and on spring flow from Salado Springs, located midway between Lyman Lake and St. Johns

(Montgomery and Associates, 2019). The water table of the aquifer around St. Johns and Lyman Lake is near the surface; historically, groundwater has discharged from the aquifer into the river and lake (Hart et al., 2002).

The groundwater and surface springs near the Cedar Mesa anticline, also known as St. Johns dome, contain high levels of HCO_3^- due to the migration of dissolved CO_2 from the St. Johns gas field (Moore et al., 2003; Gilfillan et al., 2011). The extensive travertine deposits in the Springerville-St. Johns area, particularly between Lyman Lake and Salado Springs, formed as CO_2 -enriched groundwater emerged from springs and rapidly precipitated calcium carbonate (Crumpler et al., 1994; Moore et al., 2003, 2005). However, the outflow rate of CO_2-enriched waters and, by extension, the precipitation of travertine has decreased significantly over time, likely due to a decrease in the hydraulic head and the decreasing elevation of the water table (Crumpler et al., 1994; Moore et al., 2005; Priewisch et al., 2014).

The Cedar Mesa anticline is a broad, asymmetrical anticline that spans 1,800 km^2 and trends northwest, with an axis that plunges to the northwest and the southeast (Figure 1) (Rauzi, 1999; Stevens and Tye, 2007; ADEQ, 2016). It is bounded on the southwest by the Coyote Wash fault, which has normal displacements ranging from 30 meters (m) at Salado Springs to 200 m at the apex of the anticline (Rauzi, 1999; Embid, 2009; ADEQ, 2016). Within the anticline, portions of the Supai Formation (composed of Permian red-bed clastic rocks, and carbonates), as well as the fractured basement of pink, Precambrian crystalline granite, form a CO_2 gas reservoir (Allis et al., 2001). The reservoir is relatively shallow, located 200–700 m below the surface, with an average depth of 600 m (Allis et al., 2001; Stevens and Tye, 2007). The overlying impermeable clays, mudstones, and anhydrite beds, along with the anticline structure itself, create the seal (Rauzi, 1999; Allis et al., 2001). The gas exists in discontinuous, vertically isolated reservoirs separated by thin, localized anhydrite and mudstone seals (Moore et al., 2005; Stevens and Tye, 2007). An estimated 393 billion cubic meters (m^3) of CO_2 exist as free gas in the reservoir (Stevens and Tye, 2007). Although CO_2 is the primary gas in the reservoir, at

concentrations of 83–99% (an average of 92%) of the total gas composition, nitrogen (6.6%), helium (0.6%), and argon (0.2%) also occur. The concentrations of these gases vary spatially within the dome (Stevens and Tye, 2007). Based on the helium-isotope composition of the gas, the CO_2 was derived from a mix of crustal and magmatic sources, with as much as 20% of the helium originating from the mantle (Gilfillan et al., 2008; Priewisch et al., 2014).

The CO_2 reservoir is characterized as insecure, meaning that leakage of CO_2 to the surface has occurred in recent geologic time (Miocic et al., 2016). The location of the travertine deposits indicates that the Coyote Wash fault zone is the primary pathway for CO_2 transportation to the surface (Embid, 2009; Keating et al., 2013; Priewisch et al., 2014; Miocic et al., 2019). Additionally, the helium isotope ratios ($^3He/^4He$) identified along the Coyote Wash fault and at the north tip of the fault near Salado Springs indicate transport and mixing of magmatically derived CO_2 and noble gases typically only found at depth (Gilfillan et al., 2011). This indicates that upward transmission of CO_2 likely occurs along the fault damage zone, aided by the fault's extensional nature, which allows for greater connectivity than compressional faults (Hart et al., 2002; Gilfillan et al., 2011). Water chemistry and strontium isotope measurements by Keating et al. (2014b) indicate that CO_2 from the Precambrian basement dissolves in brine from the Supai Group before moving upward along the fault, where it mixes with shallow, fresh groundwater. Yet, despite increased water extraction near the fault over the last several decades, the groundwater salinity has not increased, possibly due to the large horizontal area of the fault zone, which makes brine intrusion less likely (Keating et al., 2013; Montgomery and Associates, 2019).

The Coyote Wash fault and Cedar Mesa anticline play a significant, yet poorly understood role in the relationships between the St. Johns gas field, groundwater flow, and the travertine deposits. The TEP SGS has several groundwater production wells in the Coyote Wash fault zone. On the downthrown, southwest side of the fault, these wells have high yields and minimal drawdown (Keating et al., 2014a). The upthrown, northeast side of the fault is thought to be a hydrologically distinct zone since (1) wells there experience minimal measurable drawdown and (2) the Kaibab Limestone is dry on the east side of

the Coyote Wash fault at previously drilled wells (Keating et al., 2014a; ADEQ, 2016). A groundwater flow model by Keating et al. (2014a) tested variables to determine the depth of the Coyote Wash fault zone in conjunction with the permeability of the Glorieta Sandstone, the San Andreas Limestone, and four units of the Supai Formation. Their best-fit conceptual model characterized the Coyote Wash fault as a deep, permeable, and discrete hydrologic zone (Keating et al., 2014a).

Recent literature has described the Cedar Mesa anticline axis as a fault, in addition to the Coyote Wash normal fault (Embid, 2009; Keating et al., 2014a). This interpretation is based on borehole records from Rauzi (1999) that indicate faulting at depth, as well as personal communication with T. White referenced in Embid (2009). Recent groundwater-monitoring reports generated by Montgomery and Associates (2019) for SGS follow this interpretation. In addition, drilling and groundwater monitoring along the Cedar Mesa anticline in the SGS well field have revealed conditions suggesting that (1) the hinge acts as a barrier to lateral groundwater flow and (2) it might contain offset structures similar to a fault (J. Hammond, TEP, verbal commun., 2019). Initial field work in 2019 used a line of geophysical surveys over the Cedar Mesa anticline to examine whether any small-offset faults were visible in the subsurface. However, the survey line was not completed over the entire zone of interest and further fieldwork was indefinitely delayed due to the COVID-19 pandemic. Therefore, additional interpretation of the structural features of the Cedar Mesa anticline and the potential faulting along its axis are beyond the scope of this study. Hereafter, the feature is exclusively referred to as an anticline, but the reader should bear in mind that it may have some characteristics of a fault.

1.2 Research Objectives

A model was created to map the subsurface geology of the Springerville-St. Johns area using borehole lithologic records and groundwater flow in the area, with particular attention given to the interaction between flow, the Coyote Wash fault, and the Cedar Mesa anticline axis. The primary study objective was to determine whether currently observed groundwater-flow conditions could be replicated by including the Cedar Mesa anticline axis as a horizontal barrier to flow. If so, what is the

corresponding rate of groundwater flow across both the Coyote Wash fault and the Cedar Mesa anticline axis? Do these geologic structures act as barriers to flow or do they channel flow in a particular direction? How do the active pumping wells at SGS affect the flow in the C-aquifer? The study also examined what the borehole data can indicate about the subsurface geology in the area.

2. METHODS

A steady-state groundwater model for the area was developed using the United States Geological Survey (USGS) MODFLOW code, using the Groundwater Modeling System (GMS) version 10.4.6 for pre- and post-processing.

2.1 Conceptual Model

The boundary conditions for the model were defined as a general head boundary (GHB) and no-flow boundaries. A GHB assumes that water flows across the boundary because of a head difference at a distant source, mediated by the conductance of intermediate materials. Initially, watershed boundaries were retrieved from the USGS (2018) Watershed Boundary Dataset. A study-area boundary was selected based on a local sub-watershed level (described as hydrologic unit code 12 in the Watershed Boundary Dataset) surficial boundary that included the TEP power plant and Lyman Lake. However, the established direction of groundwater flow, as described in previous reports (Mann and Nemecek, 1983; Montgomery and Associates, 2019), did not correspond to the surficial watershed boundary. A second attempt used the Little Colorado River as a west boundary, but the Little Colorado River did not appear to act as a proper barrier to flow. The final boundary conditions were determined using flow contours from the Montgomery and Associates (2019) water monitoring report (Figure 3). The south and southeast boundaries are assumed to be general head boundaries, whereas the east and west boundaries intersect the flow contours at right angles and are therefore parallel (no-flow) boundaries. The north boundary is a general head boundary.

The Coyote Wash fault and the Cedar Mesa anticline axis were digitized based on their drawn locations in the Montgomery and Associates (2019) report (Figure 3).

Recharge values were estimated as Precipitation − Evapotranspiration. Evapotranspiration was calculated using averaged Normalized Difference Vegetation Index (NDVI) data for the study area in conjunction with the formula from Goulden et al. (2012):

$$Evapotranspiration = 101.49 \times [e^{2.6853 \times NDVI}]$$

NDVI data were available for the period of January 1, 2001, to January 1, 2020, in 16-day increments with a spatial resolution of 250 m × 250 m (Didan, 2015; Oak Ridge National Laboratory Distributed Active Archive Center, 2018). Precipitation data were taken from the PRISM Climate Group 30-year normals (1980–2010) at a 4 km × 4 km resolution (PRISM Climate Group, 2004) and were averaged across the entire study area in response to limited spatial variation. The data were divided into three regions using natural breaks (Jenks), and then the overall value for each section was calculated by averaging the recharge for all blocks in that subdivided region (Figure 4).

The Little Colorado River and Lyman Lake are the primary sources of surface water within the study area. Historically, both the river and the lake were considered to be gaining bodies of water (Akers, 1964; Bills et al., 1990), meaning that the aquifer was contributing to their volume. However, declines in the potentiometric head of the confined C-aquifer (Figure 5), caused by an increase in pumping to meet growing water demands, have made both the Little Colorado River and Lyman Lake losing bodies of water. Thus, the model must account for any infiltration that might also contribute recharge to the aquifer.

SGS has 14 active pumping wells in the study area (Figure 6). Location coordinates and borehole data for these wells, and others located on the SGS property, were provided by Montgomery and Associates (2016; 2019). Additional borehole data within the study area were also retrieved from the Arizona Department of Water Resources (ADWR) (1980) Registry of Wells in Arizona (Wells 55) database. All wells and boreholes were digitized based on their approximate location according to the georeferenced SGS Monitoring Map, or according to the recorded cadastral in the ADWR Wells 55 registry. Their locations were further refined using tax parcel information and aerial imagery.

Digital elevation model (DEM) data were obtained from the USGS (2017) 3D Elevation Program at a resolution of 1/3 arc-second (approximately 10 m). The surface elevations of wells and boreholes were determined by using the USGS DEM to create a triangulated irregular network (TIN) to which the points were snapped. Measurements for the boreholes, recorded in feet below land surface, were converted to meters. The DEM TIN was then used as the land surface level with reference to all geologic contact measurements.

Borehole information was used to characterize the subsurface geologic unit contacts. A total of 42 borehole records were compiled for the study (Figure 7). The subsurface geology was grouped into five units based on the descriptions from the drill logs in the borehole records: Alluvium/Cenozoic deposits, the Chinle and Moenkopi Formations, the Kaibab Limestone, the Coconino Sandstone, and the Supai Formation. Samples of drill cuttings were incomplete for two wells (CCR-2U and CCR-1D), resulting in greater uncertainty for these data points. Unit contacts in CCR-1U are based on a gamma-ray log as opposed to the typical drill-cutting samples.

By plotting the original borehole records in the model, it was determined that the Kaibab Limestone and Coconino Sandstone were largely consistent in their thicknesses across the study area, despite some regional deformation and subsurface structures. This analysis aligns with the description of the subsurface geology in Akers (1964) and Mann and Nemecek (1983). For boreholes where drilling did not extend for the entire depth of the aquifer unit, the missing horizon contacts were synthesized. This ensured that the geologic units in the model, particularly the Coconino Sandstone and the upper part of the Supai Formation (Upper Supai), were not falsely truncated due to a shallower termination depth of drilling (Table 1). The Upper Supai layer was extended to a depth of 40 m, the estimated maximum depth of its aquifer connectivity before the unit grades into impermeable siltstone and evaporite deposits (Mann and Nemecek, 1983). The original boreholes and modified boreholes were then combined in a dataset with 19 interpolated boreholes (Figure 6) generated from initial data and located around the model boundary. Through inverse-distance weighting of this dataset, and by

representing missing horizons implicitly, a solid (3D volumetric representation) of the study area's stratigraphy was created in GMS. For each borehole, the top elevation was set to the DEM TIN and the bottom elevation was set to the idealized bottom of the borehole. Cross sections of the solid were created to visualize the model's subsurface geologic unit contacts (Figure 8).

2.2 Numerical Model

After reviewing the available data, it was decided that the MODFLOW model would function best as a two-layer system, made by combining the upper two units into a confining layer and the bottom three units into an aquifer layer. Scatter-point layers were extracted for the bottom of the solid model, Horizon 4 (the contact between the Kaibab Limestone and the Chinle and Moenkopi Formations, representing the boundary between the aquifer and the upper confining layers), and the top of the model. A two-layer 3D grid was generated to align the "i" axis with the strike of the Coyote Wash fault and Cedar Mesa anticline (northwest to southeast) (Figure 9), facilitating the creation of a linear hydraulic flow barrier. The top and bottom elevations for the cells in each layer were interpolated from the scatter points extracted from the solids. Since Layer 1 represents a frequently unsaturated confining layer, the MODFLOW-NWT solver was used to accommodate the large quantity of cells that went dry where the water table was below the Layer 1.

Because the conceptual model indicated that the north and south boundaries of the model needed to be general head boundaries, these boundaries were created using the MODFLOW General Head package (GHB) (Figure 10). GHB input parameters include the stage and conductance. Starting values for the stage were estimated based on observed heads from nearby observation points. The north boundary was assigned a uniform starting stage of 1,615 m, whereas the south boundary was assigned a starting stage of 1,870 m at the west edge, 1,900 m where it intersects with the Coyote Wash fault, and 1,967 m east of the Cedar Mesa anticline; this variation accounts for the changes in head elevation seen across the different zones. The conductance for both the north and south boundaries was set at 1 square meter per day per meter ($[m^2/d]/m$).

The MODFLOW Horizontal Flow Barrier (HFB) package was used to create a horizontal barrier to flow along a sequence of vertical MODFLOW grid cell walls most closely aligned with the Coyote Wash fault and Cedar Mesa anticline (Figure 10). Flow across a barrier (Q) is calculated as the head drop (ΔH) across the barrier multiplied by a hydraulic characteristic (HC) equal to the hydraulic conductivity (K) divided by the horizontal thickness of the barrier (T) (Aquaveo, 2022):

$$Q = HC \times \Delta H$$

$$HC = \frac{K}{T}$$

The initial hydraulic characteristic for both the Coyote Wash fault and Cedar Mesa anticline was 0.00001 in response to the hypothesis that both acted as barriers to lateral flow.

The starting values for hydraulic conductivity were selected based on generalized hydraulic conductivity values according to the geology of each layer as outlined in Heath (1983). For Layer 1, a value of 0.0001 meters per day (m/d) was chose given the presence of both shale and alluvium. For Layer 2, a value of 5.0 m/d was chose given the presence of both carbonate rocks and sandstone in the aquifer. These initial values were applied uniformly across their respective layers.

The recharge zones and their respective estimated values, discussed previously, were entered into the model using the Recharge (RCH) package in MODFLOW.

The Little Colorado River was included in the model using the MODFLOW River (RIV) package (Figure 10). The parameters for the RIV package include stage and bottom elevation (both assigned to nodes along the river arc) and conductance (assigned along the length of the arc). The Little Colorado River was divided into two arcs: one upstream of Lyman Lake and one downstream of Lyman Lake. Nodes were located at the start and end points of the arcs, with an additional node placed at the location of the Salado Springs stream gage. The input values for the nodes and a description of the data used is presented in Table 2.

The stage values along the Little Colorado River were based on the available average stream-gage height for the recorded years (Table 2). The output of Lyman Lake did not have a stream gage, so

instead, its stage was estimated using the DEM ground elevation at the approximate start point, which was identified using Google Earth imagery. Since the downstream gage for the Little Colorado River above Zion Reservoir was outside the study area, data were initially input and the model was allowed to interpolate between the points. A point at the edge of the boundary was then selected and the model-generated head value was used. The stream-bottom elevation was calculated by assuming the thickness of riverbed sediments to be 5.18 m, in turn based on measurements at the Little Colorado River Dam site, which is located downriver from the study area, past St. Johns (Spicer, 1940).

Conductance for the river arcs can be calculated using the following formula (modified from Aquaveo, 2019):

$$C_{cell} = \frac{K * A}{M} = \frac{K * L * W}{M}$$

Where (K) is the hydraulic conductivity of the riverbed material and (A) represents the area, which can be subdivided into the width of the river (W) and the length of the of the arc as it overlaps with a cell (L), which is calculated in automatically in MODFLOW. The thickness of the riverbed sediments is represented by (M) and was initially estimated assuming an approximate thickness for river-bed sediments of 5.18 m (Spicer, 1940). Spicer's report also established that the river-bottom sediments were predominantly wet clay; therefore, a hydraulic conductivity of 8.65×10^{-7} m/d was used to calculated estimated starting values. The stream was estimated, through sampling at random intervals along the study extent using Google Earth imagery, to be an average of 7 m wide above Lyman Lake and 4 m wide below Lyman Lake. Thus, starting conductance values were estimated to be 1.16×10^{-6} $(m^2/d)/m$ for the Little Colorado River arc upstream of Lyman Lake and 6.66×10^{-7} $(m^2/d)/m$ for the Little Colorado River arc downstream of Lyman Lake.

Lyman Lake was input into the model using the MODFLOW GHB package (Figure 10). For general head polygons, conductance (C_{poly}) is calculated as:

$$C_{poly} = \frac{k}{t}$$

Where k is the hydraulic conductivity of the lake-bottom sediments and t is the thickness of the lake-bottom sediments. Initial calculations for k were calculated based on values for wet clay using the thicknesses of riverbed sediments reported in Spicer (1940), resulting in an initial conductance value of 1.67×10^{-7} square meters per day (m^2/d). Gage data was available for Lyman Lake for water years 1991–2009, 2018, and 2019. The average head during this time was calculated to be 1,816 m; this value was input for the stage of the lake.

Pumping data for SGS production wells was available for 1985–2018 (Montgomery and Associates, 2019). Not all wells were in production for the entire timespan; thus, each well's pumping rate was averaged based on their years in operation (Table 3). These values were added to MODFLOW as extraction wells (Figure 10).

Since complete groundwater-monitoring data were only available for a single time period, the model was run as a steady-state simulation.

2.3 Calibration

The model was calibrated using groundwater-monitoring levels from 46 monitoring wells, measured in January 2019 and published in the Montgomery and Associates (2019) hydrogeologic monitoring program report. These values were input as observation points across the study area (Figure 11). The calibration process continued until the model-generated head values aligned with the observed head values. Initial adjustments indicated that the river was not directly connected to the primary aquifer; thus, observed river-flow data were eliminated as reference points.

The head and conductance values assigned to the general head boundaries on the north, south, and southeast boundaries were iteratively refined during the calibration process. The hydraulic characteristic values for both the Coyote Wash fault and the Cedar Mesa anticline were determined by iteratively changing the values until the modeled head loss across the barrier matched the head loss measured in the field.

Hydraulic conductivity was adjusted during the calibration process via a combination of iteratively selected zones and pilot points. Layers 1 and 2 were each divided into two zones, determined based on observation points that responded similarly to changing conditions (Figure 12). Within each of Layer 2's zones, a set of pilot points with different minimum and maximum values was used to calibrate the hydraulic conductivity of the aquifer. The area between the Coyote Wash fault and the Cedar Mesa anticline axis, henceforth referred to as the "fault zone," contained 50 scatter points, chosen with adaptive placement. The area outside the fault zone contained 41 scatter points, also chosen with adaptive placement. The values for these scatter points were then adjusted and re-interpolated to the grid cells via inverse model runs with PEST (parameter estimation), turning them into pilot points that have model-estimated values. The values from these pilot points were then interpolated to estimate the hydraulic conductivity around the points, allowing for the representation of anisotropic variability.

Recharge was refined in the established zones using parameter estimation during model calibration. Additionally, the isolated elevated region in the western section was incorporated into the surrounding region based on the model response (Figure 4).

During initial model runs, the calculated conductance for the Little Colorado River was determined to be too low. In response, a hydraulic conductivity of 0.03 m/d and a river-bed sediment thickness of 2 m were used to calculate an upstream conductance of 0.1042 $(m^2/d)/m$ and a downstream conductance of 0.0599 $(m^2/d)/m$.

Similarly, the initial values for the hydraulic conductivity and the thickness of the lake-bottom sediments were quickly determined to be far too low and thick, respectively. Instead, conductance values ranging from 0.015 square meters per day per square meter $([m^2/d]/m^2)$ to 0.000015 $(m^2/d)/m^2$ were iteratively input before selecting 0.00009 $(m^2/d)/m^2$ as the final conductance value.

2.4 Particle Tracking

Once the groundwater model was fully calibrated, particle tracking under present-day and historical conditions was simulated using MODPATH, a particle-tracking post-processing model.

Particle tracking allows for a more detailed examination of how water particles move through an aquifer over time. The parameters required to run particle tracking include (1) creating points at a location, (2) designating the number of particles generated in each cell, (3) assigning the placement of particles within each cell, (4) specifying the duration of the particle tracking, and (5) defining the effective porosity for each layer in the model (which affects particle travel times). From there, tracking can be run forward to see where particles travel relative to their creation locations, or backward to see where particles might have originated to result in them terminating at their creation locations. The duration can run "to end," which tracks the particles for an unlimited timespan until they reach a final destination within the model, or a time range can be designated to show the maximum distance that particles can travel within a set period under the modeled conditions. Output for each particle includes a line of travel, the time taken to reach the maximum extent of travel, and the cell coordinates of the ultimate location.

Due to the usage of MODFLOW-NWT and its known compatibility issues with dry cells, the dry cells in Layer 1 were inactivated to allow MODPATH to run successfully. Since those cells were effectively disconnected from the underlying aquifer under present conditions, this change had no effect on the model calibration.

The effective porosity of the Layer 2 aquifer was set at 17.5% for the aquifer based on experimental results for Coconino Sandstone (Ma et al., 2014), though similar values were reported for the C-aquifer units in Sass et al. (1982) and Shomaker (1971). Porosity values for the geologic units making up the confining Layer 1 were also reported by Sass et al. (1982); for this study, a value of 0.5% was selected to represent the impermeable characteristics of the layer's effective porosity.

The calibrated model represented present day pumping conditions with active pumping wells. To simulate historical pre-pumping conditions, the calibrated model was altered to shut off all pumping wells. This was the only variable changed between the pumping and pre-pumping conditions for particle tracking. Since there were no groundwater monitoring observation point data available for pre-pumping

conditions, the pre-pumping model could not be independently calibrated and, therefore, is likely less accurate than the calibrated pumping model.

Six particle sets were created at different locations, as described below. Particle Sets B through F were run with the calibrated model to represent present-day pumping conditions, as well as with pre-pumping model to represent historic conditions. Particle Set A involved particles placed at the pumping wells, so that set was only run in the calibrated pumping model.

Particle Set A included 20 points placed around each of the 14 extraction wells. Two tracking runs were produced, both under present-day pumping conditions: one backward to the particles' beginning points and one backward for a duration of 13,514.25 days (representing the approximate 37 water years between 1985, when pumping began, and 2023).

Particle Set B included 36 points placed on the water-table surface in each of the Layer 1 cells containing the lake. Three tracking runs were produced: one forward to the particles' modeled end points under present-day conditions, one forward for a duration of 13,514.25 days under present-day conditions, and one forward to the particles' modeled end points under pre-pumping conditions.

Particle Set C included 18 particles generated within each cell, with cells selected one row east of the Cedar Mesa anticline axis along its full extent. Two tracking runs were produced, running forward to the particles' modeled end points under present-day conditions and pre-pumping conditions.

Particle Set D included 18 particles generated within each cell, with cells selected in the fault zone between the Cedar Mesa anticline axis and the Coyote Wash fault. Two tracking runs were produced, running forward to the particles' modeled end points under present-day conditions and pre-pumping conditions.

Particle Set E included 18 particles generated within each cell, with cells selected around the south border of the model. Two tracking runs were produced, running forward to the particles' modeled end points under present-day conditions and pre-pumping conditions.

Particle Set F included 18 particles generated within each cell, with cells selected across the area east of the Cedar Mesa anticline axis. Two tracking runs were produced, running forward to the particles' modeled end points under present-day conditions and pre-pumping conditions.

3. RESULTS

3.1 Calibrated Model Results

The final calibrated results for head contours are presented in Figure 13 along with the observation points and their error bars. The residuals between the observed and calculated head values are shown in Figure 14. Based on the available data, the model is considered to be well-calibrated. The statistical values for the calibrated model are shown in Table 4.

The hydraulic characteristic values for the structures were determined to be 1.0 for the Coyote Wash fault and 0.0001 for the Cedar Mesa anticline (Table 5).

Calibrated hydraulic conductivity values are shown in Figure 15. The hydraulic conductivity in Layer 1 was consistently low throughout all calibrations. The final calculated values for the two zones are 0.969×10^{-1} meters per day (m/d) for Zone 1 and 0.325×10^{-2} m/d for Zone 2. Layer 2 had a much greater range in hydraulic conductivity values calculated with pilot points, particularly in the fault zone, where the values are highest. The hydraulic conductivity range for the fault-zone pilot points was set as 0.0001−40.0 m/d. For pilot points located outside the fault zone, the hydraulic conductivity range was set as 0.01−20.0 m/d. Calculated pilot point values in Zone 3 are shown in Table 6 and those in Zone 4 are shown in Table 7.

The recharge values determined through the calibration process were several orders of magnitude lower than the starting input values (Table 8).

All other values calculated during the model calibration are also presented in Table 5.

3.2 Particle Tracking Results

3.2.1 Particle Set A

When allowed to run under present-day pumping conditions with no time limit, the particle tracking analysis for Particle Set A (representing the wells) shows that the starting locations for roughly two-thirds of the particles originate in the groundwater of Layer 2 (Figure 16). The remaining one-third of the particles originated in Layer 1, the majority of which came from the vicinity of the present-day Little Colorado River and Lyman Lake. The maximum travel time for particles originating in Layer 2 is 1,222,129 days or 3,346.01 years, the minimum travel time is 134,988 days or 369.58 years, and the average travel time is 279,103 days or 764.14 years. The average and minimum travel times are considerably shorter in Layer 2 than in Layer 1, where the particles have an average travel time of 510,737 days or 1,398.32 years and a minimum travel time of 287,852 days or 788.10 years. The maximum travel time for Layer 1 particles, 1,176,634 days or 3,221.45 years, is more comparable to that of Layer 2 particles.

Given that all these travel times exceed the amount of time that pumping has occurred at these wells, the duration of the particle tracking was then shortened to 13,514.25 days or about 37 water years. This is the approximate length of time between when pumping began in 1985 and the present day (2023). During this shortened timespan, the particles captured by the wells originate entirely within the Layer 2 groundwater (Figure 17). The majority (80%) of the particles start upgradient of the wells at a higher elevation and are pulled down to the wells, whereas the remaining 20% start downgradient of the wells at a lower elevation and are pulled up to the wells.

3.2.2 Particle Set B

When run with no time limit under present-day conditions, Particle Set B (the particle-tracking analysis for Lyman Lake) shows that the ending location for 94% of the particles is in Layer 2, with an average travel time of 440,711 days or 1,206.60 years (Figure 18). The minimum travel time for particles ending in Layer 2 is 163,251 days or 446.96 years, whereas the maximum travel time is

9,844,355 days or 26,952.38 years. The remaining 6% of particles terminate in Layer 1 near the current downstream flow path of the Little Colorado River. These particles have an average travel time of 255,092 days or 698.41 years. The minimum travel time is 215,711 days or 590.59 years, whereas the maximum travel time is 284,890 days or 779.99 years.

When the duration of particle tracking is shortened to 13,514.25 days, the distance particles travel is severely curtailed. All particles stay near the lake and the primary direction of movement takes the form of changes in elevation (Figure 19). Over the span of the 37 water years of pumping, the lake particles travel down an average of 14.7 m, with a minimum drop in elevation of 0.09 m and a maximum of 34.2 m.

Under pre-pumping conditions, Particle Set B has a predominantly upward migration trend. The particles increase an average of 15.08 m in elevation, with a minimum elevation increase of 4.14 m and a maximum increase of 40.08 m (Figure 20). Since there is little lateral movement, the travel times range from a minimum of 10.86 days to a maximum of 15,436 days or 42.26 years. The average travel time is 409 days or 1.12 years.

3.2.3 Particle Set C

Under pumping conditions, a strong pull from the pumping wells draws particles across both the Cedar Mesa anticline axis and the Coyote Wash fault, as well as pulling back some particles that were downgradient (Figure 21). Twenty-five percent of the particles continue downstream and flow out of the model without crossing the Cedar Mesa anticline axis. The remaining 75% of particles cross both barriers and terminate near the pumping wells. All particles stay in the groundwater aquifer of Layer 2 and do not migrate up to Layer 1. The minimum travel time for particles is 46,272 days or 126.69 years, whereas the maximum is 1,228,380 days or 3,363.12 years. The average travel time is 264,984 days or 725.49 years.

Given pre-pumping conditions, about 27% of the particles terminate in Layer 1 near the Little Colorado River after having crossed one or both faults while traveling through the zone of high

hydraulic conductivity. The particle transit time to the Layer 1 end points averages 412,595 days or 1,129.62 years, with a minimum travel time of 15,699 days or 42.98 years and a maximum of 1,237,516 days or 3,388.13 years. Travel times are higher for the particles remaining in Layer 2, at an average of 525,304 days or 1,438.21 years. The minimum travel time is a much higher 109,837 days or 300.75 years and the maximum is 1,934,627 days or 5,296.72 years.

3.2.4 Particle Set D

Similar to Particle Set C, pumping conditions for Particle Set D ensure that all the particles remain in Layer 2 except for two particles that terminate in Layer 1 near the Little Colorado River (Figure 22). Both particles travel for 39,963 days or 109.41 years. The average travel time for all remaining particles is 190,293 days or 521 years. The minimum travel time is 9,142 days or 25.03 years and the maximum is 1,121,107 days or 3,069 years.

Without the effect of the pumping wells, exactly half of Particle Set D terminates in Layer 1, predominantly in cells that intersect the Little Colorado River downstream of Lyman Lake, though some terminate at the lake itself. These particles have an average travel time of 301,742 days or 826.13 years, with a minimum travel time of 17,160 days or 46.98 years and a maximum of 1,297,849 days or 3,553.32 years. The particles that stay in Layer 2 have a slightly longer average and minimum: 340,249 days or 931.55 years and 24,228 days or 66.33 years, respectively. The maximum travel time is shorter, at only 884,793 days or 2,422.43 years.

3.2.5 Particle Set E

Particle Set E again demonstrates the influence of the pumping wells; all particles remain in the Layer 2 aquifer (Figure 23). The average travel time is 143,137 days or 391.89 years, with a maximum travel time of 1,541,339 days or 4,219.96 years. The minimum travel time, 1,031 days or 2.82 years, likely corresponds to the particles that do not flow through the model but return back out the south general head boundary east of the faults.

The particle tracking for Set E under pre-pumping conditions is useful primarily in how it demonstrates the error produced by the set general head boundary conditions once the pumping wells are turned off. Only particles on the far east edge of the model move through the system as expected; thus, the tracking times for this set are irrelevant.

3.2.6 Particle Set F

Particle Set F spans the larger area east of the Cedar Mesa anticline axis (Figure 24). Under pumping conditions, the particles all travel exclusively through the Layer 2 aquifer. The average travel time is 463,800 days or 1,269.82 years, with a minimum travel time of 82,163 days or 224.95 years and a maximum of 1,414,041 days or 3,871.43 years.

Once again, under pre-pumping conditions, some particles from Set F make their way to Layer 1 and terminate near the Little Colorado River. These particles, which represent only 5% of the overall set, have an average travel time of 571,761.22 days or 1,565.40 years, a minimum of 260,262 days or 712.56 years, and a maximum of 770,749 days or 2,110.20 years. For the other 95% of particles remaining in Layer 2, the average travel time is 432,547 days or 1,184.25 years, the minimum is 81,658 days or 223.57 years, and the maximum is 1,300,747 days or 3,561.25 years.

4. INTERPRETATION

4.1 Calibrated Model Interpretation

The particle-tracking results show that some flow likely occurs across both the Cedar Mesa anticline axis and the Coyote Wash fault. The calculated hydraulic characteristics indicate that the Coyote Wash fault is apparently not a significant barrier to horizontal flow. However, the Cedar Mesa anticline axis is three orders of magnitude more restrictive to horizontal flow than the Coyote Wash fault and two orders of magnitude more restrictive than the lows for hydraulic conductivity in the surrounding area. This could be caused by limited horizontal connectivity through the damage zone due to folding.

The resulting zone of high hydraulic conductivity between the Cedar Mesa anticline axis and the Coyote Wash fault corresponds with previous research hypothesizing that the Coyote Wash fault zone is

a broad area of high permeability (Keating et al., 2014a; Miocic, et al., 2019). The high hydraulic conductivity may also be related to overlapping damage zones from the folding in the Cedar Mesa anticline and damage zone structures from the Coyote Wash fault. Interestingly, the high permeability does not seem to run the entire southern length of the zone between the Cedar Mesa anticline axis and the Coyote Wash fault (Figure 15). Instead, the arm that extends west of the Coyote Wash fault aligns somewhat with the angle of the Buttes anticline. The Buttes anticline, located east of the northern portion of the Cedar Mesa anticline (Figure 1), is another zone of interest for future study. Miocic et al. (2019) hypothesize, on the basis of tufa mounds aligned with the fold axis, that the anticline indicates a fault in the area. However, since surficial field data and groundwater data were limited or nonexistent for this particular area, the Buttes anticline was not included in this study.

The model-calculated values for the hydraulic conductivity of Layer 1 are three orders of magnitude higher than published hydraulic conductivity values in the region, though these values are calculated exclusively for the Chinle Formation at the nearby Coronado Generating Station, located outside the study area (Nicholls, 2018). Since Layer 1 represents not only the highly impermeable layers of the Chinle and Moenkopi Formations, but also the more permeable surficial alluvium and Cenozoic deposits, the model-calculated values likely represent a true average of all the included units.

The model-calculated recharge values were significantly lower than the initially input recharge values, which were calculated from precipitation and evapotranspiration rates in the region. This makes sense in the context of the depth of the aquifer and the impermeable nature of the overlying units. Akers (1964) and Mann and Nemecek (1983) indicate that most recharge to the C-aquifer occurs in areas with exposed aquifer units, or in areas with more permeable surficial layers that lack the impermeable beds of the Chinle and Moenkopi units, and so more readily transport precipitation downwards.

4.2 Model Accuracy

4.2.1 Pumping Conditions

The model calibration achieved a high level of correspondence between the calculated and observed heads (Figure 14). Only three points exceeded the head target interval of 3 m: those corresponding to monitoring well observation points CCR-1D, CCR-1U, and CCR-2U, all of which are located within the fault zone. This area has a fairly rapid drop in head from the elevated levels east of the Cedar Mesa anticline axis to the lower drawdown areas surrounding the active pumping wells and the Coyote Wash fault. Located between the fault and the anticline axis, the area is likely a complex fold or fault damage zone with high spatial variability and rapidly changing hydraulic head elevations. These characteristics make the area difficult to model accurately given the scale of the model grid and the limited observation points.

4.4.2 Pre-Pumping

The accuracy of the pre-pumping model is diminished due to the general head boundaries on the north and south ends of the model. Thus, much of the cell flooding and the elevated water table under pre-pumping conditions would not necessarily reflect realistic conditions, since without the set boundary conditions, excess water could flow through the system. Although the proportions are likely unrealistic, we know that the C-aquifer historically contributed to the flow of the Little Colorado River and Lyman Lake due to the elevated potentiometric head of the confined aquifer (Akers, 1964; Bills et al., 1990). However, variability recorded by the gages indicates that there might be some connectivity to a perched aquifer that fluctuates seasonally.

4.3 Particle Tracking

4.3.1 Particle Set A

Not all of the wells have been pumping at their current capacity since 1985 (Table 3); thus, Figure 16 would represent a maximum range for the wells that have not operated for the entire particle-tracking runtime of 37 water years. The active pumping wells and their associated capture zones are

almost entirely located within the fault zone area of elevated hydraulic conductivity (Figure 15). This high hydraulic conductivity likely influenced the selection of the active pumping wells for SGS, given that numerous other wells drilled throughout the area by TEP are now not producing or are used as monitoring wells (Figure 3).

The results of both particle-tracking sets indicate that pumping from the SGS wells has not been ongoing for long enough to actively draw any of the water kept in Lyman Lake. Although a drawdown effect has been documented in the region since the start of pumping (Figure 5), the water used in the area appears to be entirely drawn from the C-aquifer, with minimal contributions from recharge or present-day surface waters.

Although historical pumping data were provided for the SGS wells, it would be insightful to pair the pumping rate fluctuations with the particle tracking and model analysis. At present, we do not know if the years during which a particular well pumped a lower volume of water corresponded to a reduction in the pumping capacity from that location, or if variations in well yield were merely based on the operational dynamics of the power station. Knowing whether there were significant and long-ranging changes in the production capacity of a given well would help to better understand the changing dynamics of groundwater flow in the region.

4.5.2 Particle Set B

In the time since pumping began at SGS in 1985, the particles originating from Lyman Lake have not traveled far laterally. Their particle-tracking lines indicate that infiltration to the aquifer in Layer 2 is required before lateral flow begins to occur. This corresponds to the Layer 2 aquifer acting as the primary avenue for groundwater transport and dispersion, since little transport would occur laterally through the unsaturated zones of Layer 1. Although smaller aquifer units could allow some flow in and out through Layer 1, this model indicates that the water held in the reservoir is relatively secure and is unlikely to be pulled in large quantities by pumping of the C-aquifer on any societally relevant timescale; the minimum travel time for a particle to reach the pumping wells is 446.96 years.

The pre-pumping conditions also indicate that particles from the lake do not travel far. Given the increased water in the system with the pumping wells turned off, the model indicates that the aquifer would contribute water to the lake region. Although there is greater uncertainty associated with the pre-pumping conditions and their particle-tracking results, this finding can be linked to the historic data that Lyman Lake was gaining water from the C-aquifer (Bills et al.,1990).

4.5.3 Particle Set C

The starting points for Particle Set C were aligned parallel to the Cedar Mesa anticline axis to understand how groundwater flows in its vicinity. For 75% of the length of the Cedar Mesa anticline axis, the combination of lower potentiometric heads on its west side and the pull of the pumping wells results in particles traveling across both faults to reach the active pumping sites.

Although the pumping wells increase the pull across the faults, the pre-pumping conditions for Particle Set C show a similar flow pattern; the particles preferentially travel through the zone of high hydraulic conductivity and continue onwards to outflow near the downstream Little Colorado River instead of being captured by the wells. Particles flowing out of the south border of the model are believed to be an error caused by the unaltered general head boundary conditions set in the calibrated pumping.

4.5.4 Particle Set D

The particles placed throughout the fault zone demonstrate similar tendencies to those of Particle Set C (located parallel to the Cedar Mesa anticline axis). Once again, under pumping conditions, 75% or more of these particles are captured by the wells and almost all the outflow remains in the aquifer layer, except for two particles located at the northmost grouping of particles; these two are transported to the surface of Layer 1 near the Little Colorado River.

The pre-pumping conditions show a similar pattern of flow that, despite the lack of pumping wells, moves particles through the region of high hydraulic conductivity and results in half of the particles terminating near Lyman Lake or the downstream Little Colorado River. Particles flowing out

of the south border of the model are believed to be an error caused by the unaltered general head boundary conditions set in the calibrated pumping model, although the trend occurs on a smaller scale, even under pumping conditions.

4.5.5 Particle Set E

Under pumping conditions, Particle Set E provides the best understanding of flow on the west side of the Coyote Wash fault and how water moves as it enters through the south boundary. A number of particles start on the east side of the fault, flow across the fault zone, and pass out through the southwest boundary. These indicate that this west segment of the general head boundary might be less accurate than the others and could use further refinement, since the particles would be expected to continue and flow northward through the model.

This issue is further exacerbated with the pre-pumping conditions, since none of the particles, except those in the same three northeasternmost cell blocks, continue to flow through the model. Thus, the edges of the pre-pumping model should be considered to have a lower confidence rating than the more central parts of the model.

4.5.6 Particle Set F

The results of Particle Set F allow us to delineate a clearer line for where the effect of the pumping wells and the pull across the faults extends in the east half of the model. A comparison of pumping conditions to pre-pumping conditions shows that cross-fault flow increases under pumping conditions. Yet, even without the active pumping wells, some particle-tracking lines still have similar cross-fault flow paths. The zone of high hydraulic conductivity, coupled with the lower potentiometric head on the other side of the faults, still leads to particle travel through this zone, despite the low permeability of the Cedar Mesa anticline axis. However, fewer of the pre-pumping particles from this set terminate in Layer 1 near the Little Colorado River when compared to Particle Set D. Instead, the majority of the particles continue to flow out of the system, even those that crossed the Cedar Mesa anticline axis. This likely relates to the general head boundary conditions on the north edge that were

unable to be calibrated for the pre-pumping model. The lower hydraulic head for that boundary, as established from pumping conditions, likely creates a strong head difference, given the overall higher elevation of the groundwater table elsewhere in the system.

5. CONCLUSIONS

This model of the aquifer system in the Springerville-St. Johns area of Arizona uses existing subsurface and groundwater data to deepen the understanding of the interactions between the Coconino aquifer, the Coyote Wash fault, and the Cedar Mesa anticline. Groundwater in the C-aquifer enters the study area from the south boundary of the model, flows northward, and leaves the study area via the north boundary. The area between the Cedar Mesa anticline axis and the Coyote Wash fault has a steep hydraulic gradient with flow perpendicular to the fault strike and anticline trend. Recharge to the C-aquifer in the Springerville-St. Johns area is extremely limited and is impeded by the impermeable layers of the Chinle and Moenkopi Formations. Borehole logs show that the Kaibab Limestone and the Coconino Sandstone are largely consistent in their thicknesses across the study area despite regional deformation and subsurface structures.

Results from the MODFLOW model indicate that the Cedar Mesa anticline axis behaves as a horizontal barrier to flow, whereas the Coyote Wash fault does not. However, water still crosses the Cedar Mesa anticline under pumping and non-pumping conditions. A return to the TEP SGS to complete the geophysical survey across the Cedar Mesa anticline hinge would provide additional data on the subsurface structural characteristics of the area.

A zone of high hydraulic conductivity spans the northern part of the fault zone between the Cedar Mesa anticline axis and the Coyote Wash fault. The zone also bulges out west of the fault in the area surrounding the current active SGS pumping wells; this additional arm of higher hydraulic conductivity might align with the Buttes anticline. Further investigation of the connectivity between these features would reveal more information about the nature of groundwater flow in the area.

Particle tracking for the study area indicates that pumping and the associated drawdown effect are likely reducing outflow from the aquifer system to existing surface waters, as was historically observed (Akers, 1964; Bills et al., 1990). Under simulated pre-pumping conditions, particles regularly cross the fault system and terminate within Layer 1 near the Little Colorado River and downstream of Lyman Lake. These cross-fault waters could be part of the artesian springs at Salado Springs. Thus, although outflow at the springs has diminished in recent years (Montgomery and Associates, 2019), particles from cross-fault flow could still contribute to spring discharge. Future groundwater sampling and geochemical analysis in this region, particularly in the area east of the Cedar Mesa anticline, could help validate or refine this model and would improve our understanding of the fault zone's effect on groundwater flow throughout the area.

Although SGS is responsible for the majority of groundwater withdrawals within the study area, there may be other smaller, privately owned wells pumping from the C-aquifer within the study area for which records are unavailable. Additionally, another power-generating station, Coronado Generating Station, is located just outside the study area, northeast of St. Johns, Arizona. The 2019–2020 average annual groundwater withdrawals from Coronado Generating Station are 7.03×10^6 cubic meters per year (m^3/year) (5,699 acre-feet per year [acre-ft/yr]) (Dery, 2022), less than one-third of the 2018 SGS annual pumping volume (2.32×10^7 m^3/year [18,812 acre-ft/yr]) (Montgomery and Associates, 2019). Yet, this still represents a significant quantity of water and could have an effect on the groundwater flow dynamics in the northeast corner of the model that was unaccounted for.

In conclusion, this groundwater model indicates that the Coyote Wash fault does not act as a significant barrier to horizontal flow, but that the Cedar Mesa anticline axis does act as such a barrier. The model also shows that the east side of the Cedar Mesa anticline is still hydraulically connected to the west side of the Coyote Wash fault. The area between the Cedar Mesa anticline axis and the Coyote Wash fault is a zone of high hydraulic conductivity that extends northward, as well as into an area west of the central portion of the Coyote Wash fault. These findings contribute to a deeper understanding of

the complex subsurface geology and groundwater flow dynamics of the C-aquifer across the Springerville-St. Johns area.

REFERENCES CITED

Akers, J.P., 1964, Geology and ground water in the central part of Apache County, Arizona: U.S. Geological Survey Water-Supply Paper 1771, 107 p., https://doi.org/10.3133/wsp1771.

Aldrich, M.J., and Laughlin, A.W., 1984, A model for the tectonic development of the southeastern Colorado Plateau boundary: Journal of Geophysical Research, Solid Earth, v. 89, no. B12, p. 10,207–10,218, https://doi.org/10.1029/JB089iB12p10207.

Allis, R., Chidsey, T., Gwynn, W., Morgan, C., White, S., Adams, M., and Moore, J., 2001, Natural CO_2 reservoirs on the Colorado Plateau and southern Rocky Mountains—Candidates for CO_2 sequestration: Proceedings of the 1st National Conference on Carbon Sequestration, Washington, D.C., May 14–17, 2001, 19 p.

Aquaveo, 2022, Using the MODFLOW HFB Package: Aquaveo & Water Resources Engineering News, accessed June 2023 at https://www.aquaveo.com/blog/2022/12/27/using-modflow-hfb-package.

Aquaveo, 2019, GMS: Conductance, XMS Wiki, accessed February 2022 at https://www.xmswiki.com/wiki/GMS:Conductance

Arizona Department of Environmental Quality (ADEQ), 2016, St. Johns Gas Unit (stimulated carbon dioxide wells): Arizona Department of Environmental Quality Aquifer Protection Permit 511308, 7 p., accessed July 2023 at https://www.azdeq.gov/public-notice-call-comments-app-511308.

Arizona Department of Water Resources (ADWR), 1980, Registry of Wells in Arizona (Wells 55) [database]: Arizona Department of Water Resources website, accessed August 2021 at https://gisweb3.azwater.gov/WellReg.

Bills, D.J., H. W. Hjalmarson, and Frederick N. Robertson, 1990, Estimates of Ground-water flow components for Lyman Lake, Apache County, Arizona: U.S. Geological Survey Water-Resources Investigations Report 89–4151, 55 p., https://doi.org/10.3133/wri894151.

Crumpler, L.S., Aubele, J.C., and Condit, C.D., 1994, Volcanoes and Neotectonic Characteristics of the Springerville Volcanic Field, Arizona, *in* Chamberlin, R.M., Kues, B.S., Cather, Barker, J.M., and McIntosh, W.C., eds., Mogollon Slope, West-Central New Mexico and East-Central Arizona: New Mexico Geological Society 45th Annual Fall Field Conference, September 28–October 1, 1994, Guidebook, p. 147–164, https://doi.org/10.56577/FFC-45.

Dery, J.L., 2022, Water usage for power generation & opportunities for water reuse expansion—A study of Salt River Projects water usage: Tucson, Arizona, University of Arizona, master's thesis, 139 p., accessed July 2023 at https://hdl.handle.net/10150/665413.

Didan, K., 2015, MOD13Q1—MODIS/Terra Vegetation Indices 16-Day L3 Global 250m SIN Grid V006 [database]: National Aeronautics and Space Administration Level-1 and Atmosphere Archive & Distribution System Distributed Active Archive Center website, accessed July 2023 at https://ladsweb.modaps.eosdis.nasa.gov/missions-and-measurements/products/MOD13Q1.

Embid, E.H., 2009, U-series dating, geochemistry, and geomorphic studies of travertines and springs of the Springerville area, east-central Arizona, and tectonic implications: Albuquerque, New Mexico, University of New Mexico, master's thesis, 103 p., accessed July 2023 at https://digitalrepository.unm.edu/eps_etds/26/.

Gilfillan, S.M.V., Ballentine, C.J., Holland, G., Blagburn, D., Lollar, B.S., Stevens, S., Schoell, M., and Cassidy, M., 2008, The noble gas geochemistry of natural CO_2 gas reservoirs from the Colorado Plateau and Rocky Mountain provinces, USA: Geochimica et Cosmochimica Acta, v. 72, no. 4, p. 1174–1198, https://doi.org/10.1016/j.gca.2007.10.009.

Gilfillan, S.M.V., Wilkinson, M., Haszeldine, R.S., Shipton, Z.K., Nelson, S.T., and Poreda, R.J., 2011, He and Ne as tracers of natural CO_2 migration up a fault from a deep reservoir: International Journal of Greenhouse Gas Control, v. 5, no. 6, p. 1507–1516, https://doi.org/10.1016/j.ijggc.2011.08.008.

Goulden, M.L., Anderson, R.G., Bales, R.C., Kelly, A.E., Meadows, M., and Winston, G.C., 2012, Evapotranspiration along an elevation gradient in California's Sierra Nevada: Journal of Geophysical Research, Biogeosciences, v. 117, no. G3, https://doi.org/10.1029/2012JG002027.

Hart, R.J., Ward, J.J., Bills, D.J., and Flynn, M.E., 2002, Generalized hydrogeology and ground-water budget for the C Aquifer, Little Colorado River Basin and parts of the Verde and Salt River Basins, Arizona and New Mexico: U.S. Geological Survey Water-Resources Investigations Report 2002–4026, 54 p., https://doi.org/10.3133/wri024026.

Heath, R.C., 1983. Basic ground-water hydrology, U.S. Geological Survey Water-Supply Paper 2220, 86p.

Jones, C.J.R., and Robinson, M.J., 2021, Groundwater and surface-water data from the C-aquifer monitoring program, northeastern Arizona, 2012–2019: U.S. Geological Survey Open-File Report 2021–1051, https://doi.org/10.3133/ofr20211051.

Keating, E., Newell, D., Dempsey, D., and Pawar, R., 2014a, Insights into interconnections between the shallow and deep systems from a natural CO_2 reservoir near Springerville, Arizona: International Journal of Greenhouse Gas Control, v. 25, p. 162–172, https://doi.org/10.1016/j.ijggc.2014.03.009.

Keating, E., Newell, D., Stewart, B., Capo, R., and Pawar, R., 2014b, Further insights into interconnections between the shallow and deep systems from a natural CO_2 reservoir near

Springerville, Arizona, U.S.A.: Energy Procedia, v. 63, p. 3195–3201, https://doi.org/10.1016/j.egypro.2014.11.344.

Keating, E.H., Newell, D.L., Viswanathan, H., Carey, J.W., Zyvoloski, G., and Pawar, R., 2013, CO_2/brine transport into shallow aquifers along fault zones: Environmental Science & Technology, v. 47, no. 1, p. 290–297, https://doi.org/10.1021/es301495x.

Ma, X., Rudnicki, J., and Haimson, B., 2014, True triaxial tests in two porous sandstones: Experimental failure characteristics and theoretical prediction: Proceedings of the 48th U.S. Rock Mechanics/Geomechanics Symposium, Minneapolis, Minnesota, June 1–4, 2014, article ARMA-2014-7286, 6 p., accessed July 2023 at https://onepetro.org/ARMAUSRMS/proceedings-abstract/ARMA14/All-ARMA14/ARMA-2014-7286/123461.

Mann, L.J., and Nemecek, E.A., 1983, Geohydrology and water use in southern Apache County, Arizona: Arizona Department of Water Resources Bulletin 1, 86 p., 5 sheets, scales 1:250,000 and 1:500,000, accessed July 2023 at https://azmemory.azlibrary.gov/nodes/view/91162.

Miocic, J.M., Gilfillan, S.M.V., Frank, N., Schroeder-Ritzrau, A., Burnside, N.M., and Haszeldine, R.S., 2019, 420,000 year assessment of fault leakage rates shows geological carbon storage is secure: Scientific Reports, v. 9, article 769, 9 p., https://doi.org/10.1038/s41598-018-36974-0.

Miocic, J.M., 2016, A study of natural CO_2 reservoirs – mechanisms and pathways for leakage and implications for geologically stored CO_2: Edinburgh, Scotland, The University of Edinburgh, PhD thesis, 302 p., accessed July 2023 at https://era.ed.ac.uk/handle/1842/17881.

Montgomery and Associates, 2016, Appendix A, construction details for new CCR monitoring wells, January–April 2016: Tucson Electric Power, prepared by Montgomery and Associates, Tucson, Arizona, 7 p.

Montgomery and Associates, 2019, Hydrogeologic Monitoring Program 2018-2019, Springerville Generating Station, Apache County, Arizona: Tucson Electric Power, prepared by Montgomery and Associates, Tucson, Arizona, 66 p.

Moore, J., Adams, M., Allis, R., Lutz, S., and Rauzi, S., 2003, CO_2 mobility in natural reservoirs beneath the Colorado Plateau and Southern Rocky Mountains—An example from the Springerville-St. Johns field, Arizona and New Mexico: Proceedings of the 2nd Annual Conference on Carbon Sequestration, Alexandria, Virginia, May 6, 2003, 22 p.

Moore, J., Adams, M., Allis, R., Lutz, S., and Rauzi, S., 2005, Mineralogical and geochemical consequences of the long-term presence of CO_2 in natural reservoirs—An example from the Springerville–St. Johns Field, Arizona, and New Mexico, U.S.A.: Chemical Geology, v. 217, no. 3–4, p. 365–385, https://10.1016/j.chemgeo.2004.12.019.

Nicholls, M., and Eshraghi, P., 2018, Coronado generating station evaporation pond liner equivalent analysis: Haley & Aldrich, Inc. Technical Memorandum 132181–003, 20 p.

Oak Ridge National Laboratory Distributed Active Archive Center, 2018. MODIS and VIIRS land products global subsetting and visualization tool [database]: Oak Ridge National Laboratory Distributed Active Archive Center website, https://doi.org/10.3334/ORNLDAAC/1379.

Priewisch, A., Crossey, L.J., Karlstrom, K.E., Polyak, V.J., Asmerom, Y., Nereson, A., and Ricketts, J.W., 2014, U-series geochronology of large-volume Quaternary travertine deposits of the

southeastern Colorado Plateau—Evaluating episodicity and tectonic and paleohydrologic controls: Geosphere, v. 10, no. 2, p. 401–423, https://doi.org/10.1130/GES00946.1.

PRISM Climate Group, 2004, Time Series Values for Individual Locations [database]: Northwest Alliance for Computational Science & Engineering website, accessed June 2020 at https://prism.oregonstate.edu/.

Rauzi, S.L., 1999, Carbon Dioxide in the St. Johns - Springerville Area, Apache County, Arizona: Arizona Geological Survey Open-File Report 99–2, 22 p., accessed July 2023 at https://library.azgs.arizona.edu/item/AOFR-1552429763526-134.

Rauzi, S.L., 2009, Implications of live oil shows in eastern Arizona geothermal test (1 Alpine-Federal), v. 2.0: Arizona Geological Survey Open-File Report 94–01, 12 sheets, scale 1:500,000, 17 p., https://library.azgs.arizona.edu/item/AOFR-1552429412492-375.

Sass, J.H., Stone, C., and Bills, D.J., 1982, Shallow subsurface temperatures and some estimates of heat flow from the Colorado Plateau of northeastern Arizona: U.S. Geological Survey Open-File Report 82–994, 112 p., https://doi.org/10.3133/ofr82994.

Shomaker, J.W., 1971, Water resources of Fort Wingate Army Depot and adjacent areas, McKinley County, New Mexico: U.S. Geological Survey Open File Report 71–1, 231 p.

Sirrine, K.G., 1958, Geology of the Springerville-St. Johns Area, Apache County, Arizona: Austin, Texas, University of Texas, Ph.D. dissertation, 247 p.

Spicer, H. Cecil, 1940, Estimate of depth to bed rock at some dam sites in the Gunnison, Little Colorado and Zuni River Basins, Colorado and Arizona based on resistivity measurements 1938-1939: U.S. Geological Survey Open-File Report 40–7, 102 p., https://doi.org/10.3133/ofr407.

Stevens, S.H., and Tye, B.S., 2007, NACS—Natural CO_2 analogs for carbon sequestration: U.S. Department of Energy, prepared by Advanced Resources International, Inc., under U.S. Department of Energy Award no. DE-FC26-01NT41150, 159 p., https://doi.org/10.2172/902517.

U.S. Geological Survey, 2017, 1/3rd arc-second Digital Elevation Models (DEMs) - USGS National Map 3DEP Downloadable Data Collection: U.S. Geological Survey National Map, accessed July 2023 at https://www.sciencebase.gov/catalog/item/4f70aa9fe4b058caae3f8de5.

U.S. Geological Survey, 2018, Watershed Boundary Dataset: U.S. Geological Survey National Map website, accessed July 2023 at https://apps.nationalmap.gov/services/.

U.S. Geological Survey and Arizona Geological Survey, 2018, Quaternary Fault and Fold Database of the United States: U.S. Geological Survey website, https://www.usgs.gov/programs/earthquake-hazards/faults.

APPENDIX

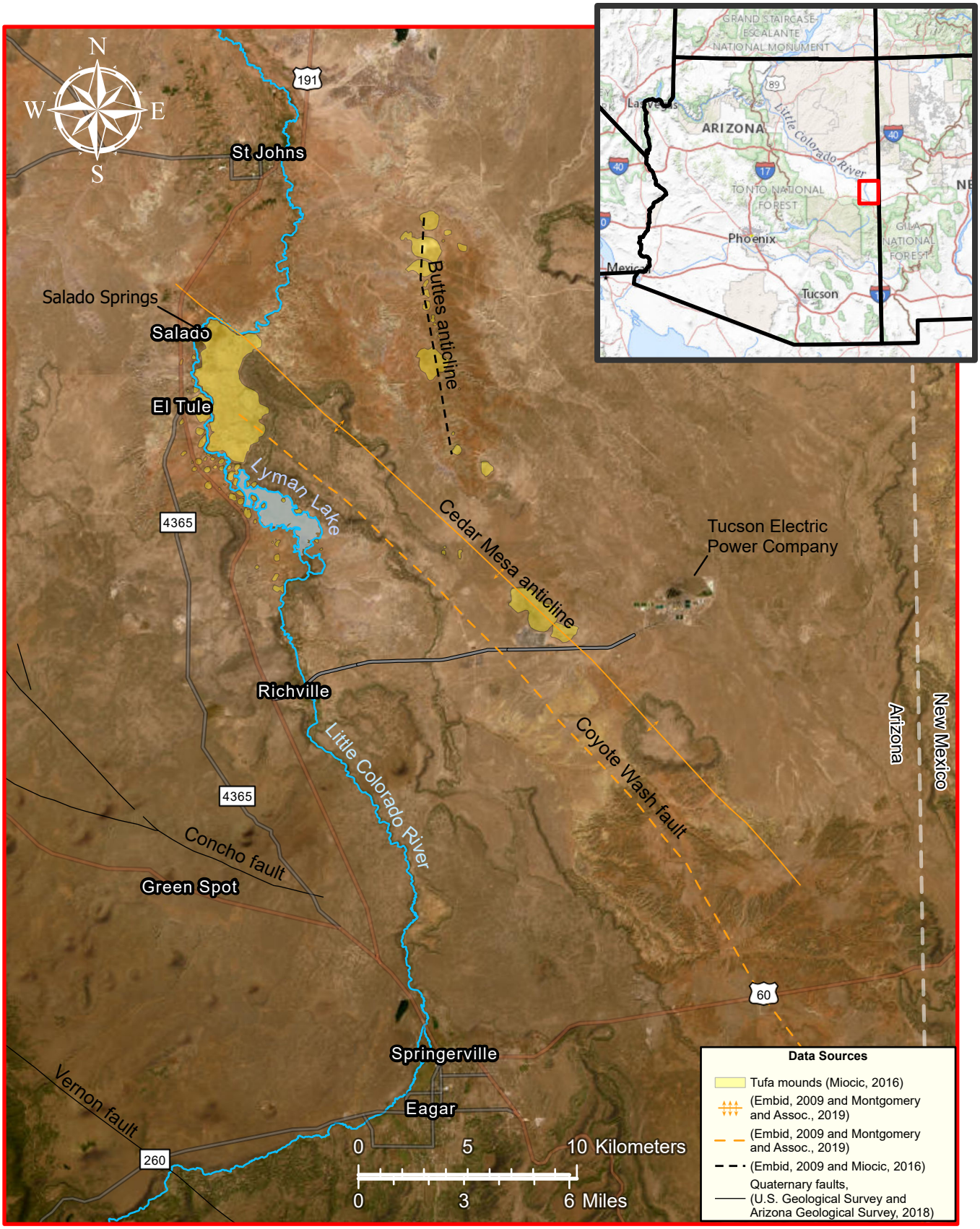

Figure 1: Overview of the St. Johns and Springerville study area showing geologic structures and their respective data sources.

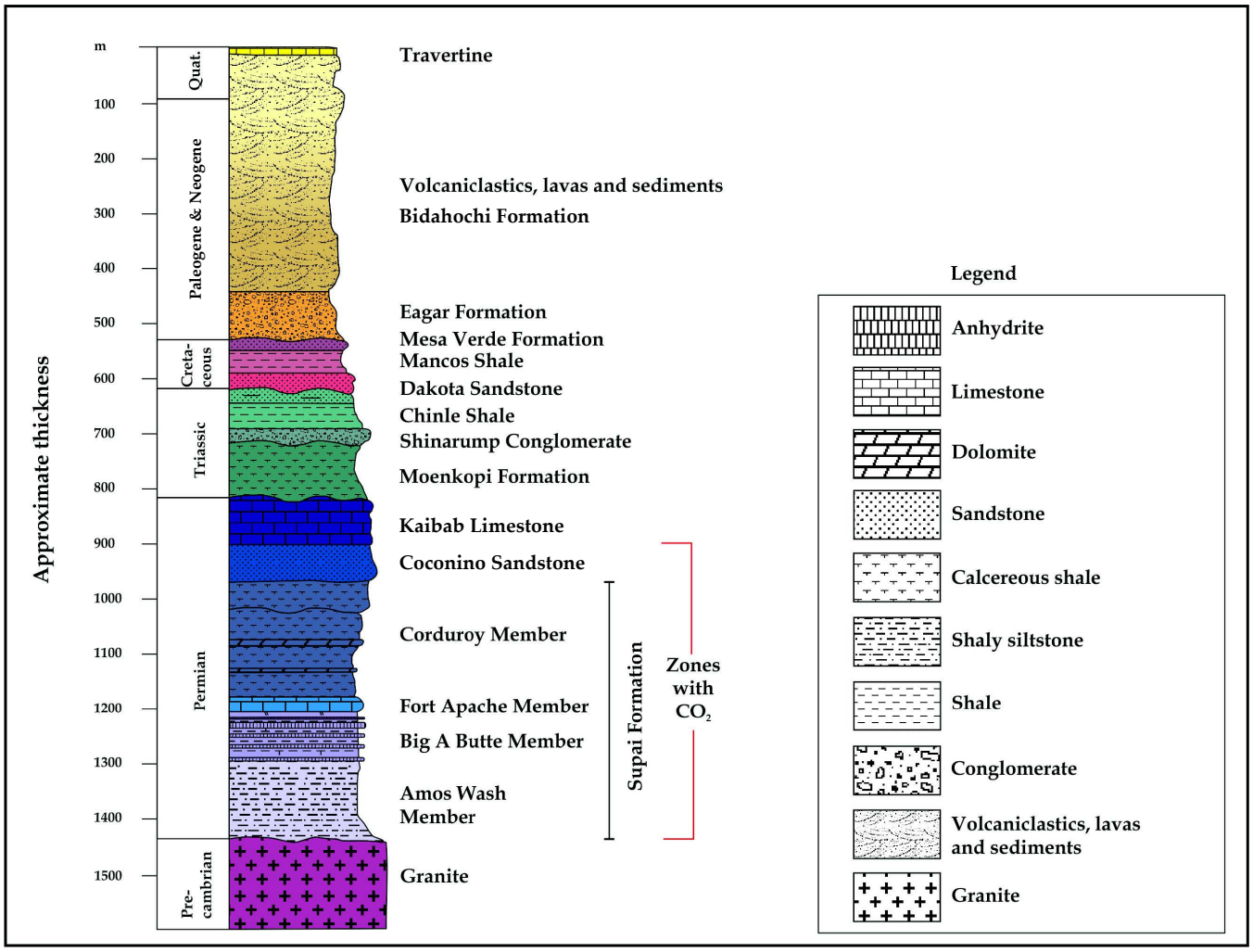

Figure 2: Idealized stratigraphy of the St. Johns-Springerville area. Deposits from the Cretaceous Period and younger can vary widely in thickness. Throughout the study area, they are often significantly thinner than represented here. Modified from Miocic (2016) after Rauzi (1999) and Embid (2009).

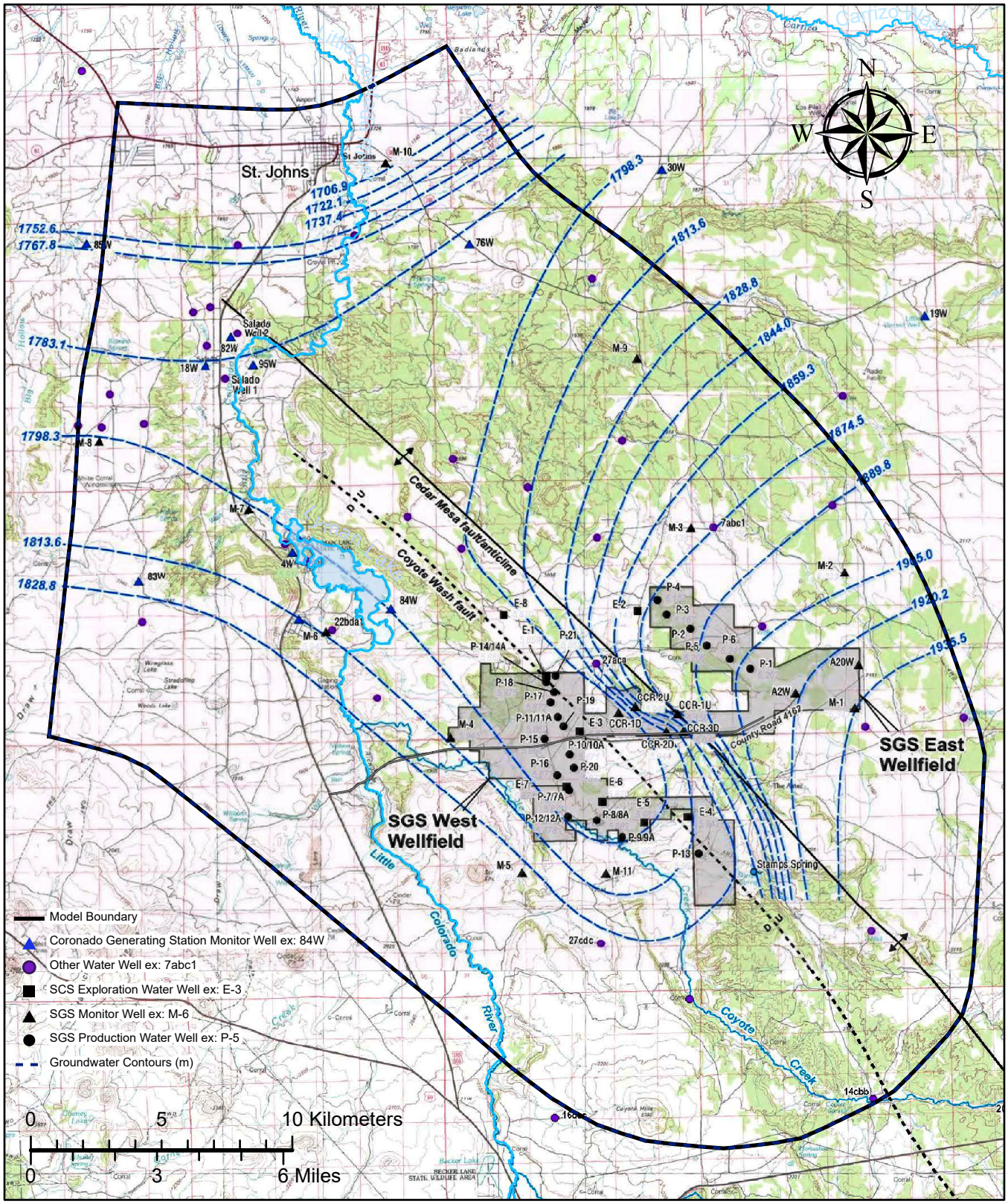

Figure 3: Model boundary conditions based on C-aquifer groundwater contour map. Modified from Montgomery and Associates (2019). Contours are in meters (m) at an interval of ~15.24 m (50 ft). Map also shows the well field of Springerville Generating Station (SGS) operated by Tucson Electric Power and associated monitoring wells described in their groundwater monitoring report.

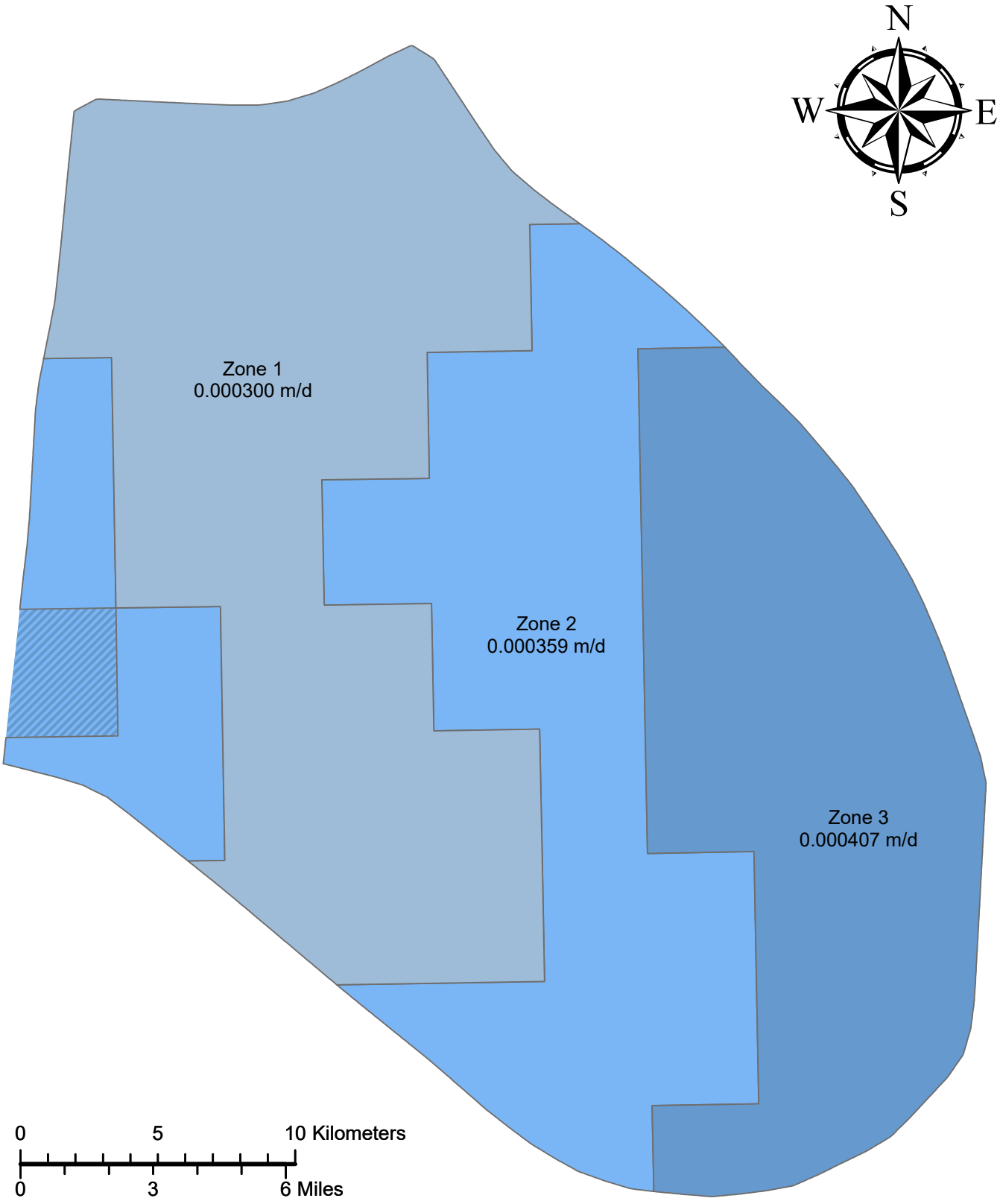

Figure 4: Starting input values for the average recharge rate. Data based on precipitation rates from the PRISM 30 year normals and evapotranspiration calculated using averaged normalized difference vegetation index (NDVI). The hatched square was initial part of Zone 3 but was later incorporated into Zone 2 based on initial calibrations.

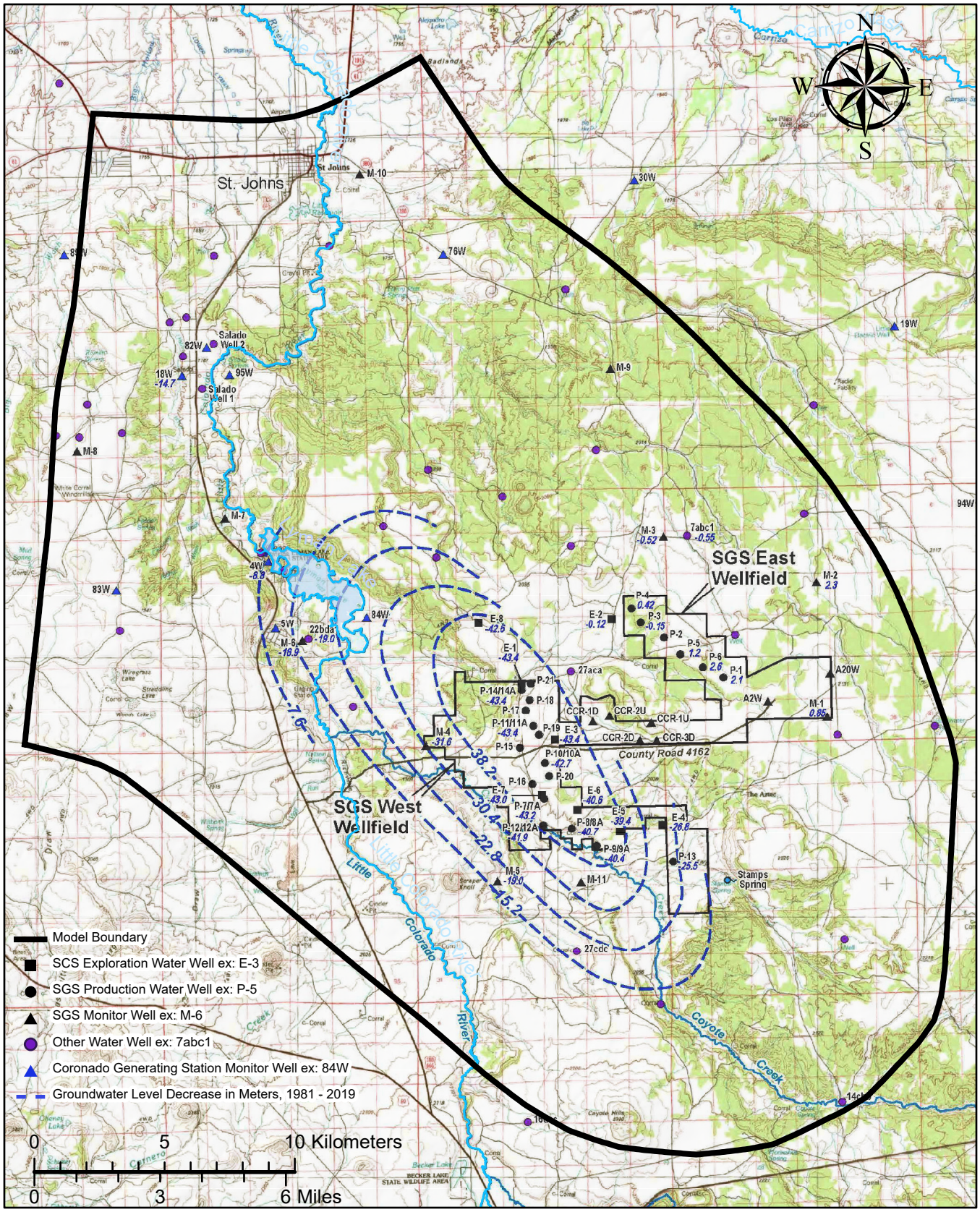

Figure 5: Documented Coconino aquifer drawdown. Modified from Montgomery and Associates (2019). Contours are in meters at an interval of ~7.6 m (25 ft). Map also shows the groundwater level change in meters from 1981-2019 at individual wells.

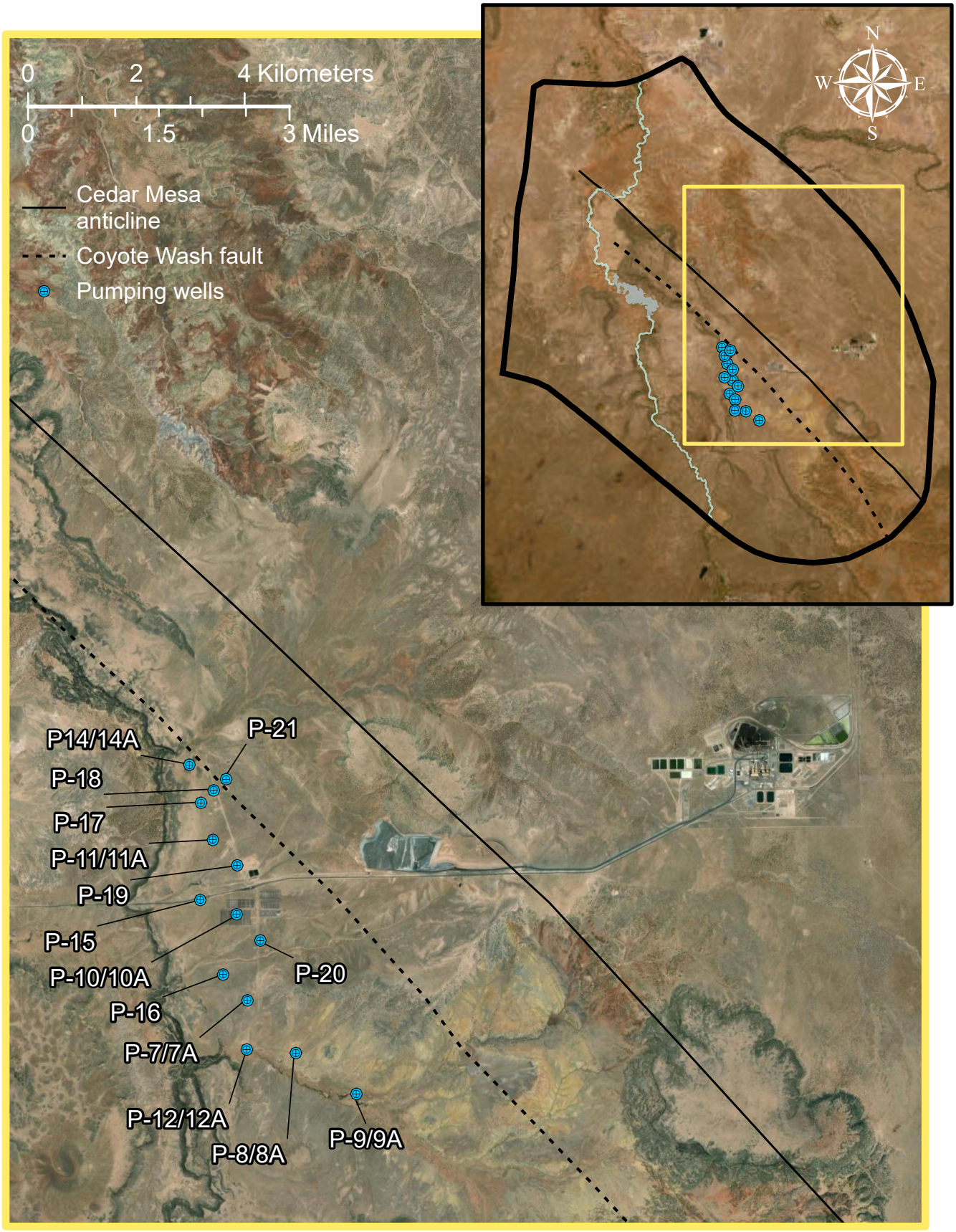

Figure 5: Location of active pumping wells at Springerville Generating Station.

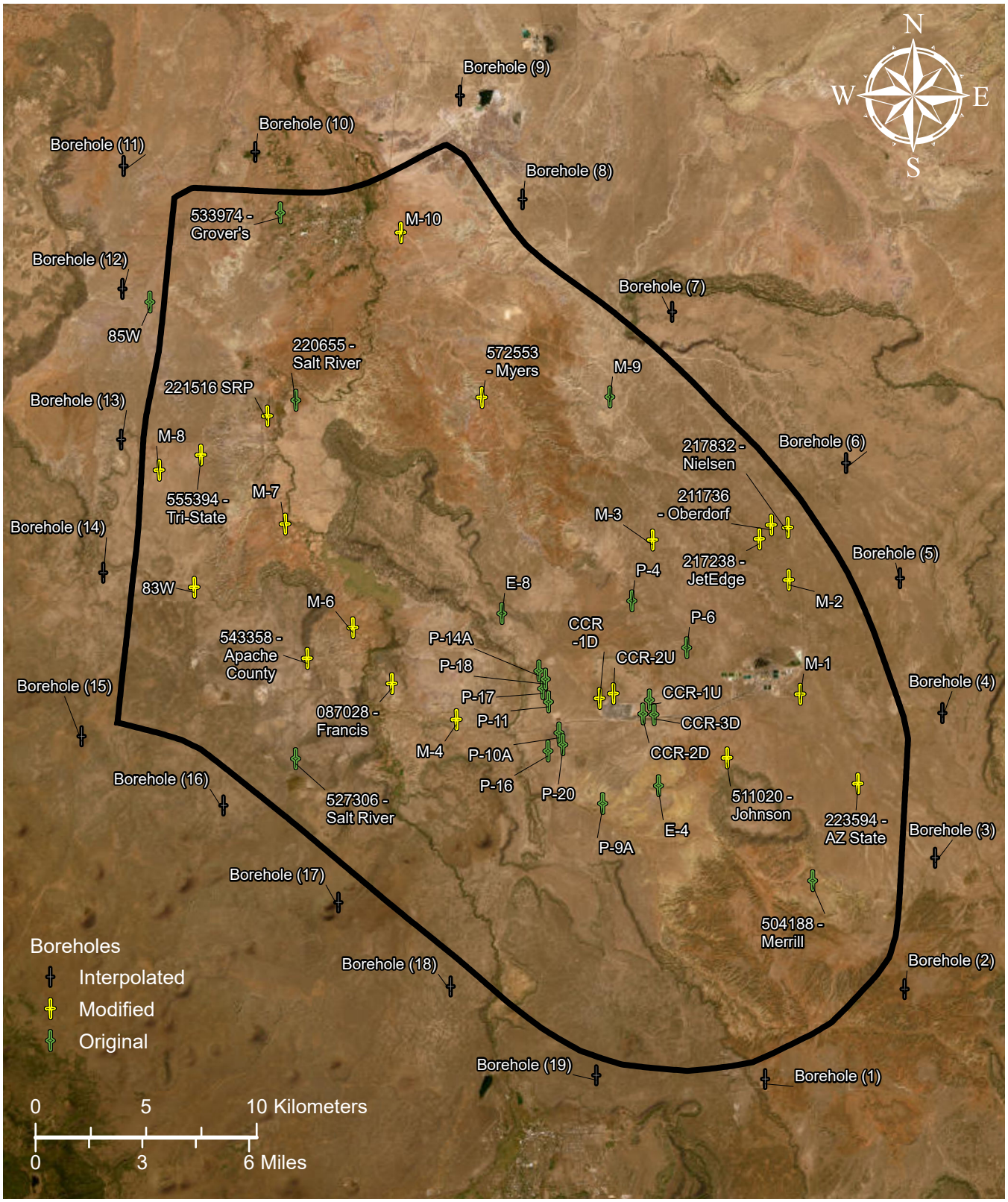

Figure 7: Borehole location and classification. Original boreholes have reliable well logs with well defined unit contacts and minimal modification. Modified boreholes have a lower confidence rating and have been adjusted to extend foreshortened units where drilling didn't extend for the entire depth of the aquifer. Interpolated boreholes were generated based on early 3D solids models created from the other borehole records.

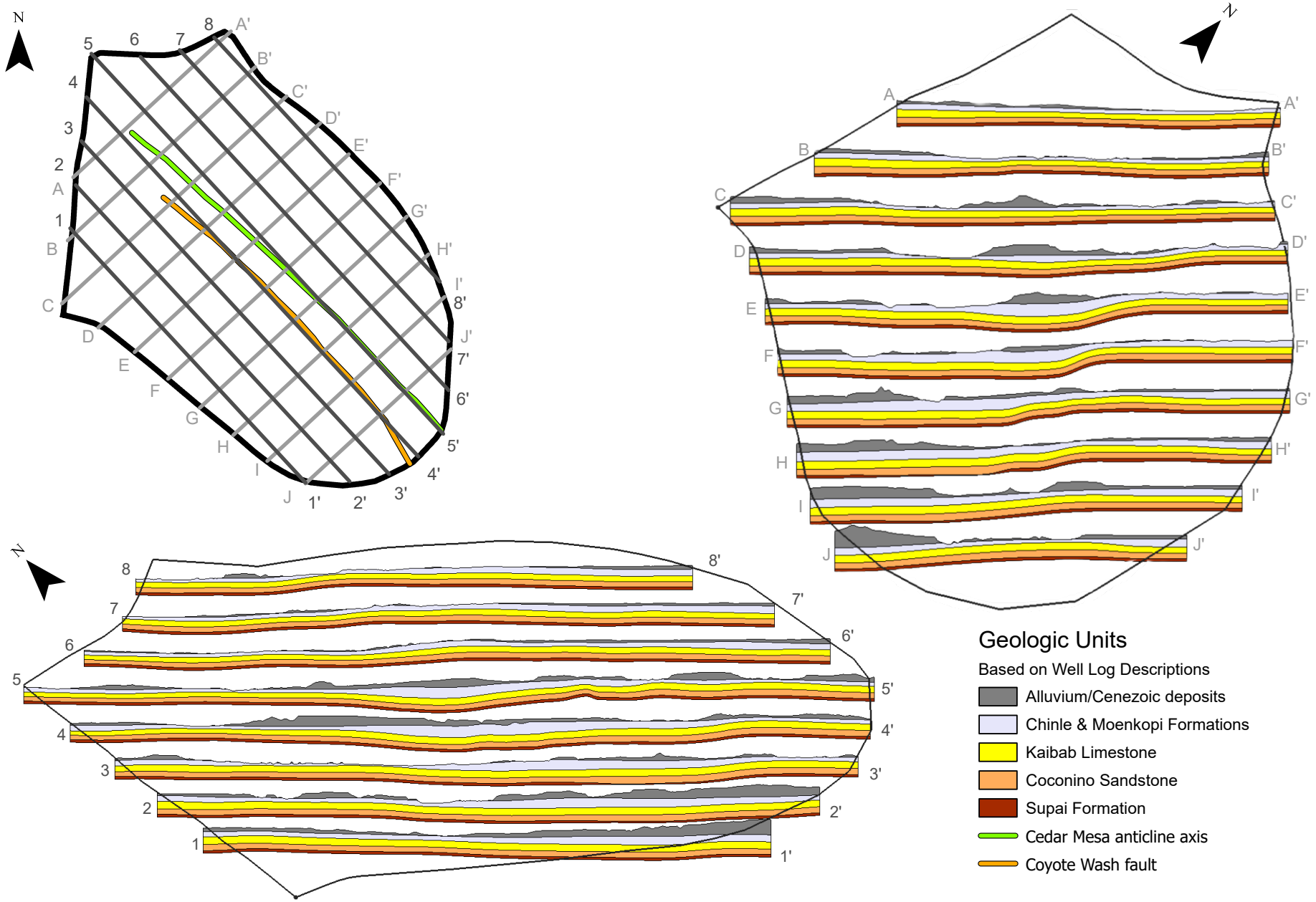

Figure 8: Stratigraphic cross sections generated from solids (3D volumetric representations) borehole data. Shown at 5x vertical exaggeration. Coyote Wash fault and Cedar Mesa anticline axis shown on overview map for reference.

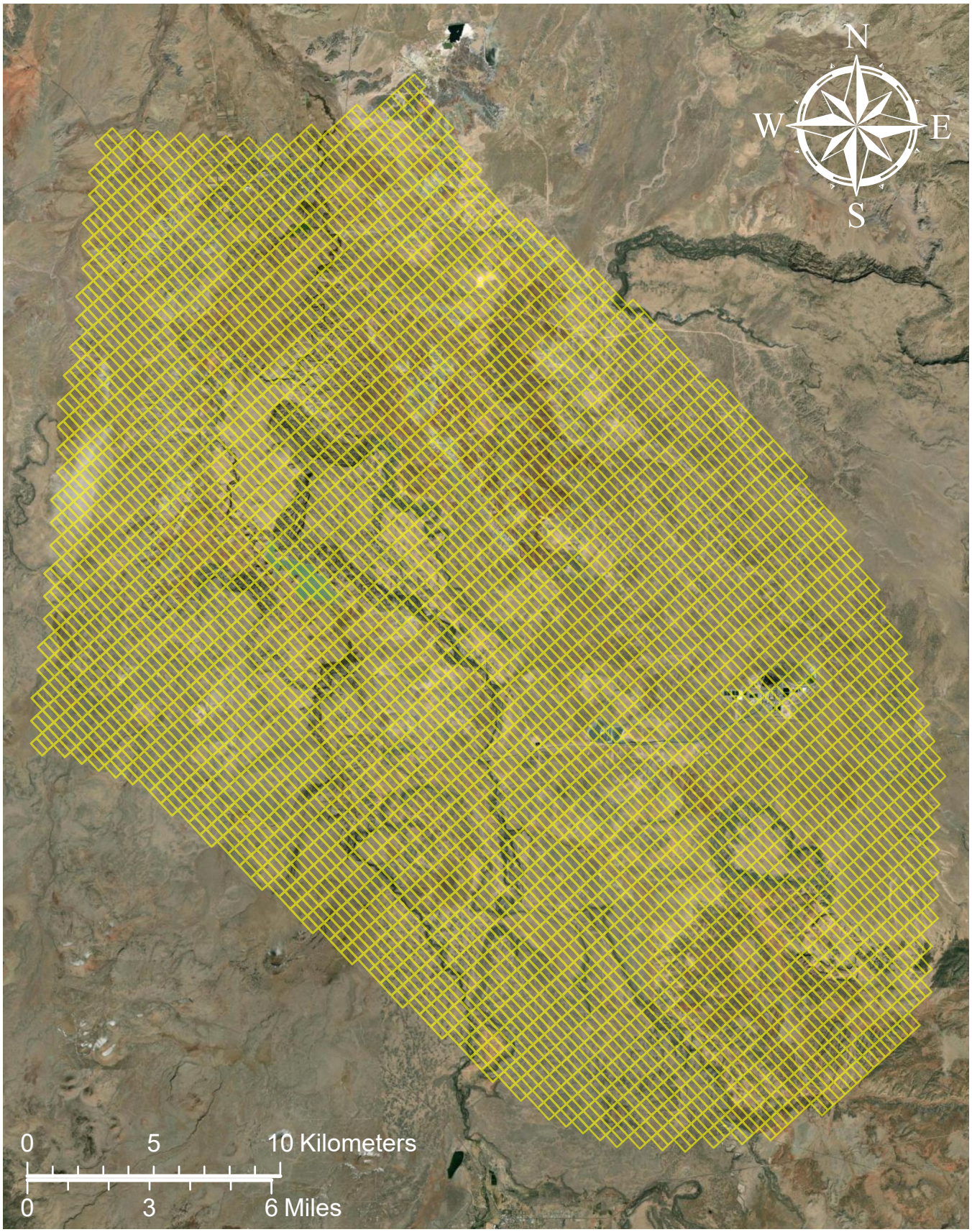

Figure 9: MODFLOW-generated two-layer 3D grid as viewed from above. Cells were oriented to align with the primary direction of the Cedar Mesa anticline axis and the Coyote Wash fault.

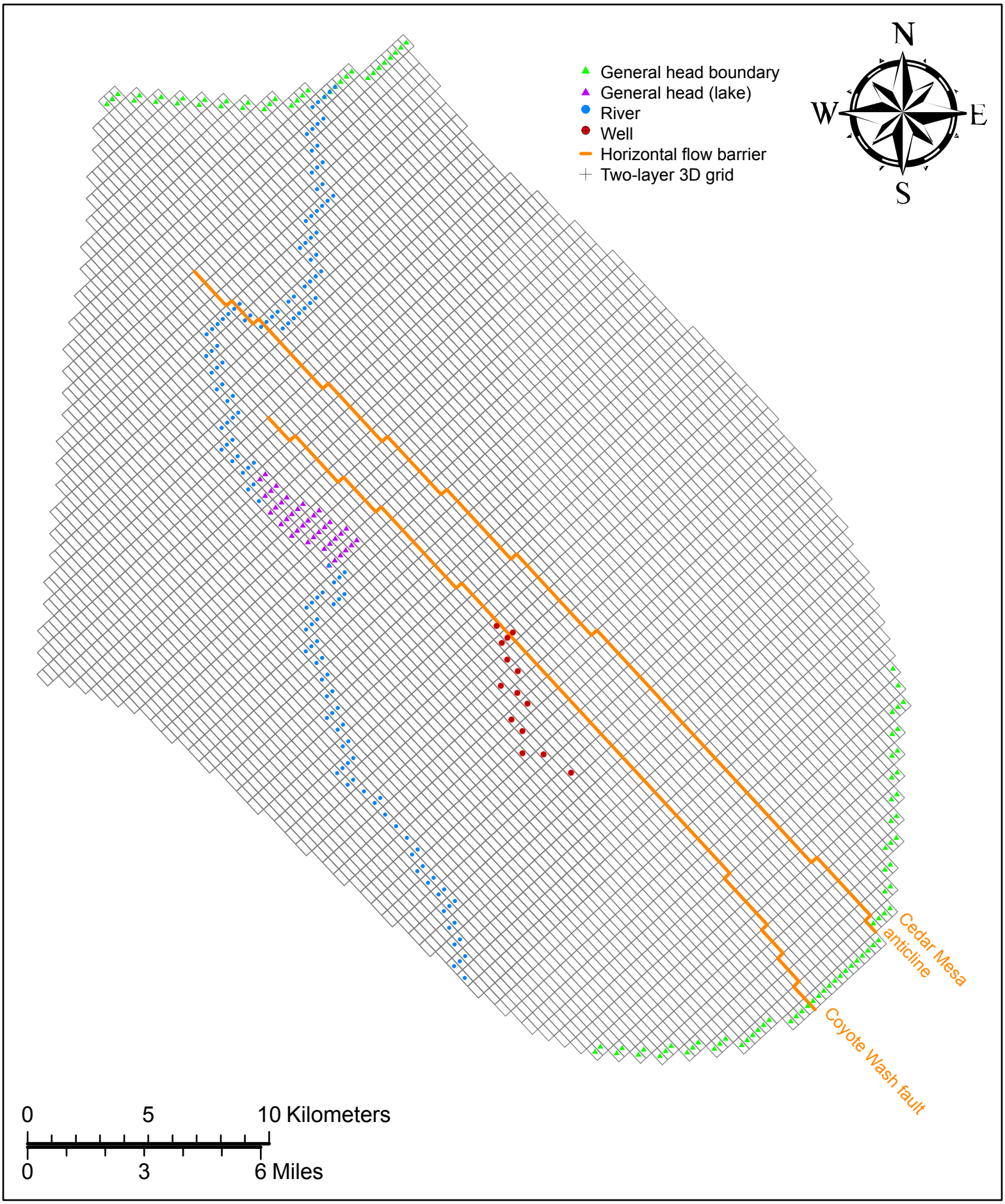

Figure 10: MODFLOW numerical model input features.

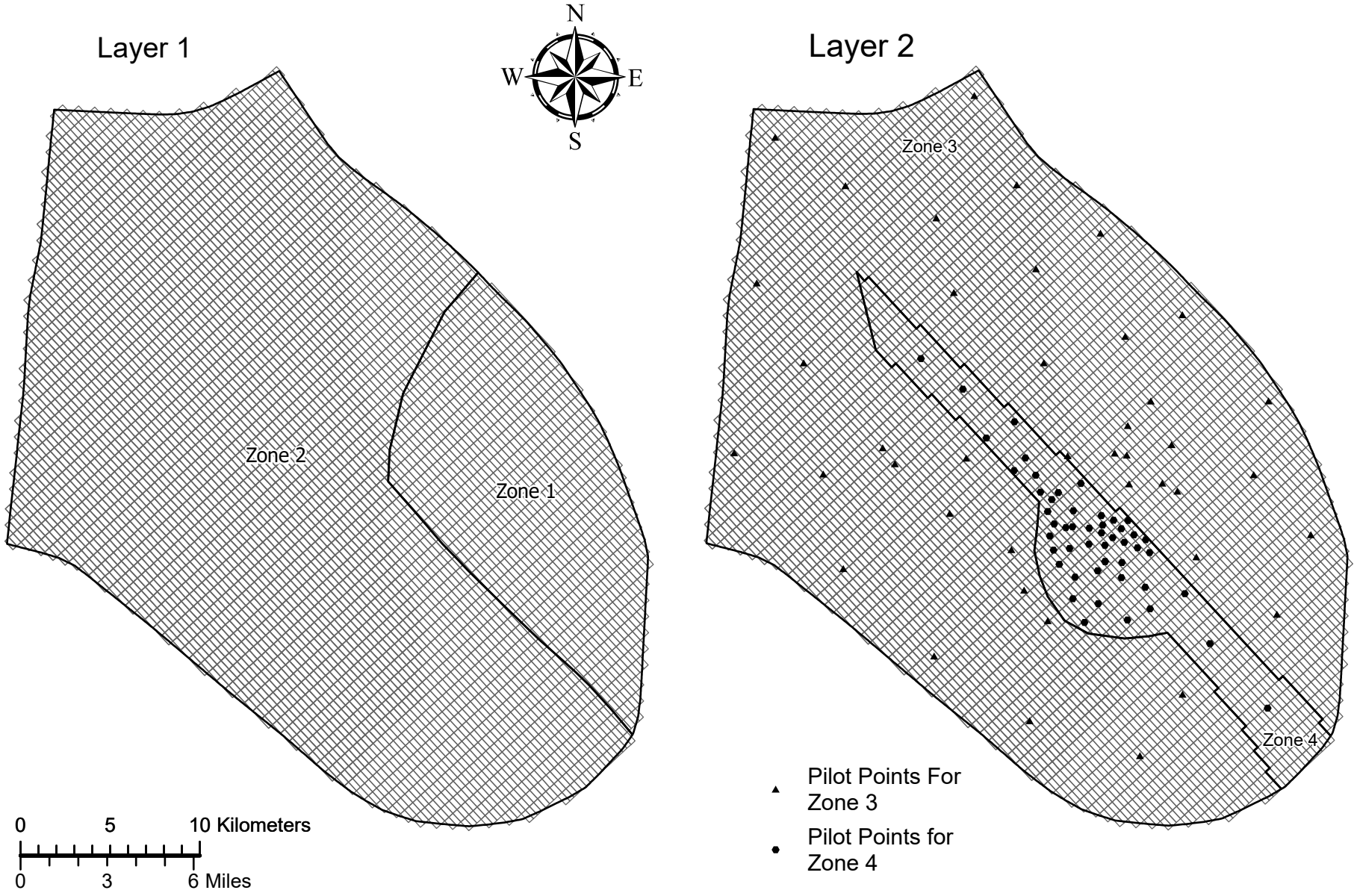

Figure 11: Hydraulic conductivity zones for Layer 1 and Layer 2 as input into MODFLOW for parameter estimation (PEST). Layer 2 utilized two sets of pilot points with differing minimum and maximum limits based on whether the points were located external to or within the fault zone.

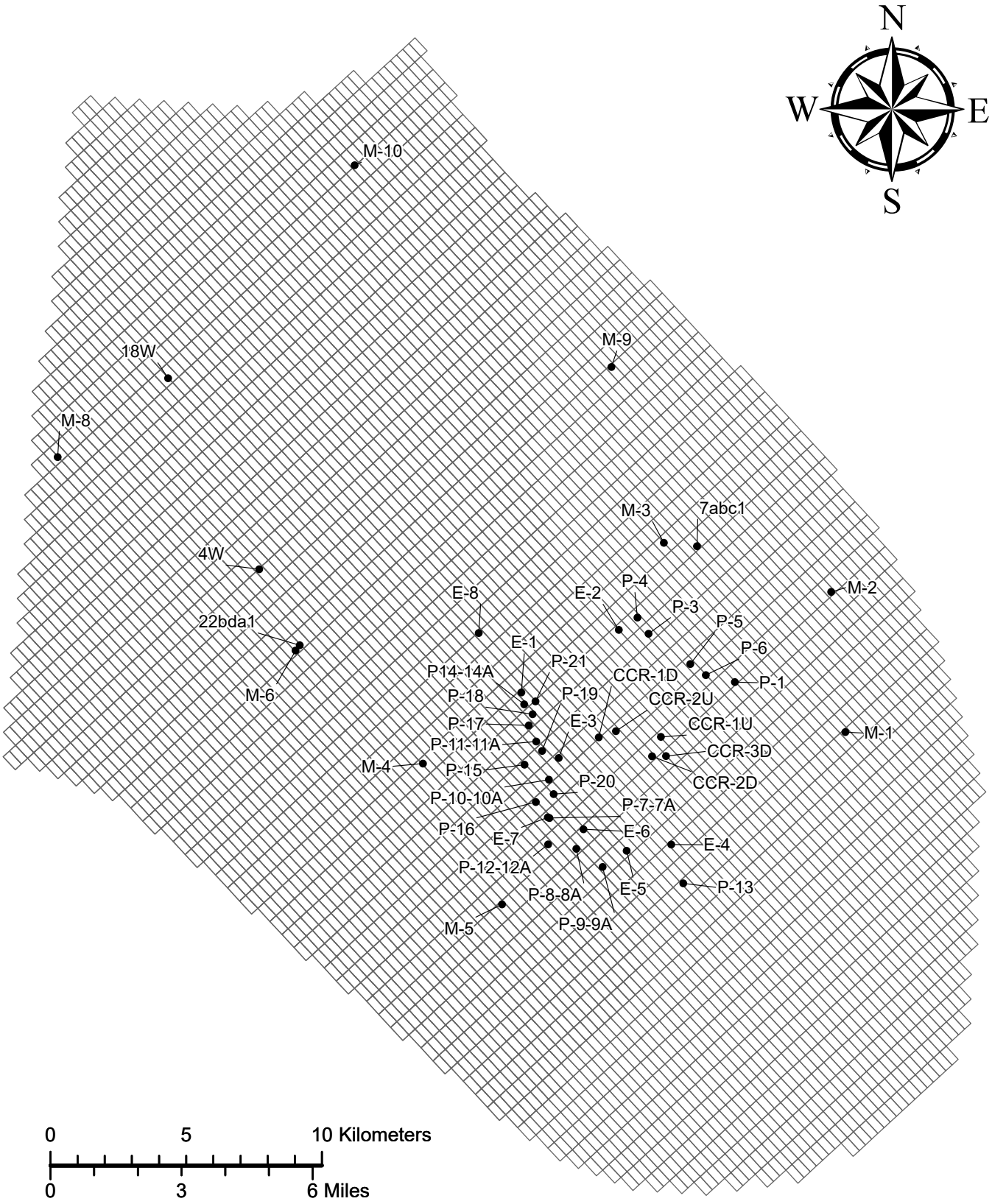

Figure 12: Monitoring well locations included as observation points in MODFLOW. Data taken from the hydrogeologic monitoring program report by Montgomery and Associates (2019).

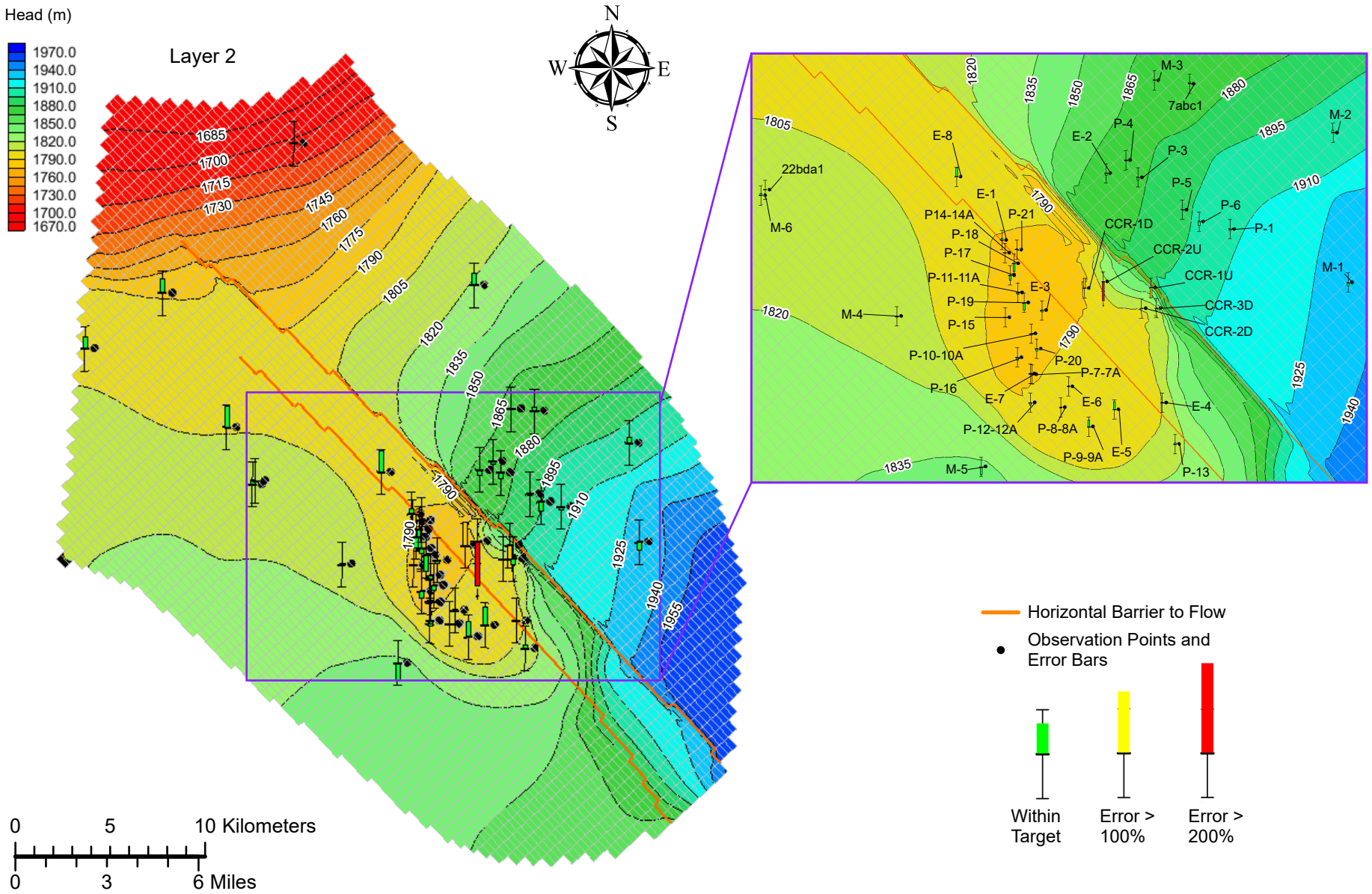

Figure 13: Head contour map for the calibrated model's aquifer in Layer 2, with observation points. The head contour interval is 15 meters. The observation point error bars have a 3-meter target interval. Coyote Wash fault and Cedar Mesa anticline axis as horizontal barriers to flow are included for reference.

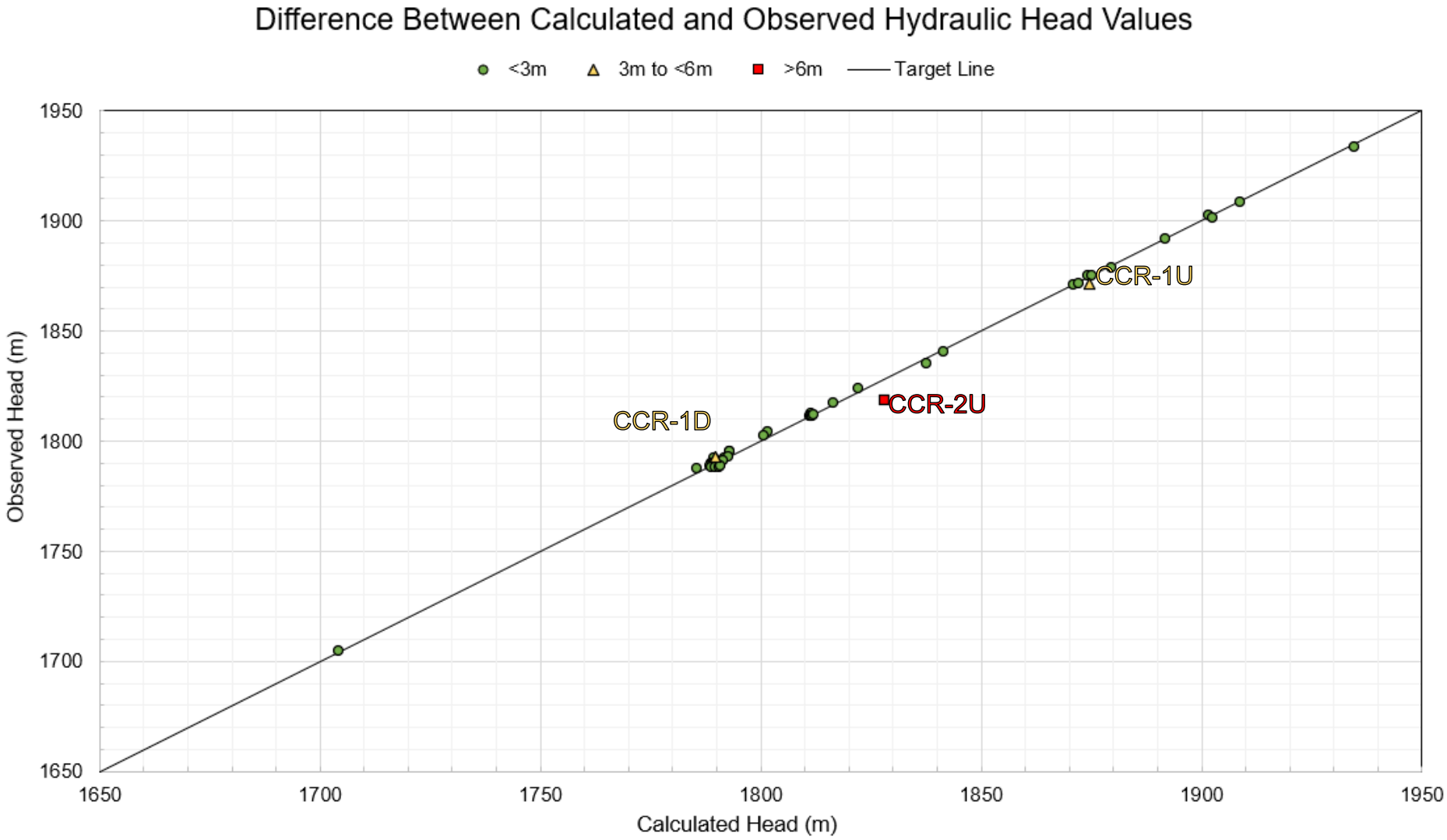

Figure 14: Plot of calculated vs observed hydraulic head values. The head target interval was 3 meters (m). Line represents a perfect match between the calculated and observed value. Green dots were within the target interval. Yellow triangles exceeded the interval but not by more than 200% or 6 m residual head. Red squares exceeded the interval by more than 200% or 6 m. Observation points that exceeded the target are labeled with the monitoring well name. The R^2 value of the line of best fit was 0.9982.

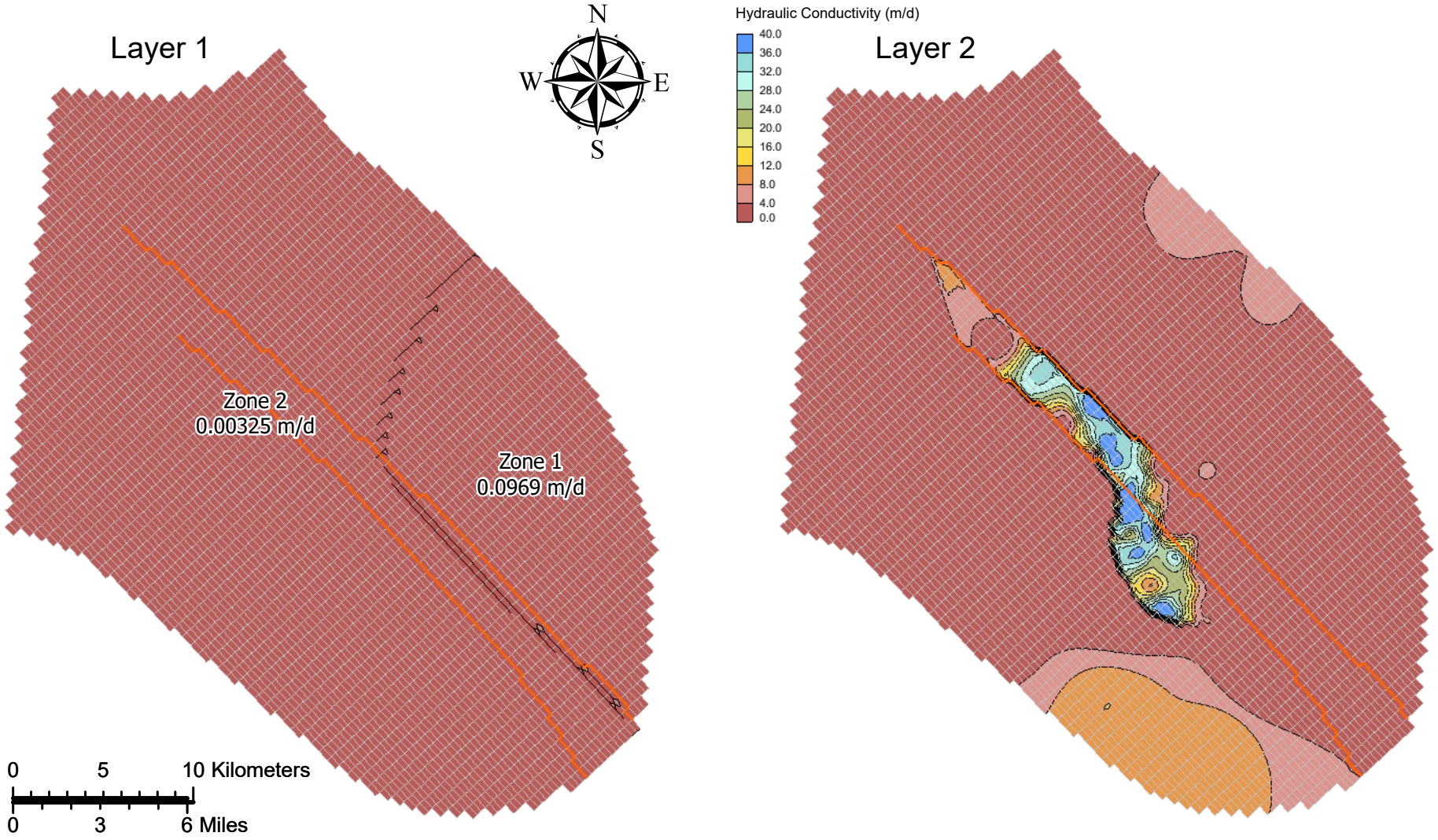

Figure 15: Hydraulic conductivity results for Layer 1 and Layer 2 calculated using parameter estimation (PEST). Layer 1 had a minimum and maximum limit of 0.0001 to 100 meters per day (m/d). Layer 2 utilized two sets of pilot points with differing minimum and maximum limits based on whether the points were located outside or within the fault zone. Limits within the fault zone were 0.0001– 40 m/d, whereas outside the fault zone, the limits were 0.01–20 m/d. These limits were determined iteratively based on model response. The Coyote Wash fault and Cedar Mesa anticline axis, used as horizontal barriers to flow, are included for reference.

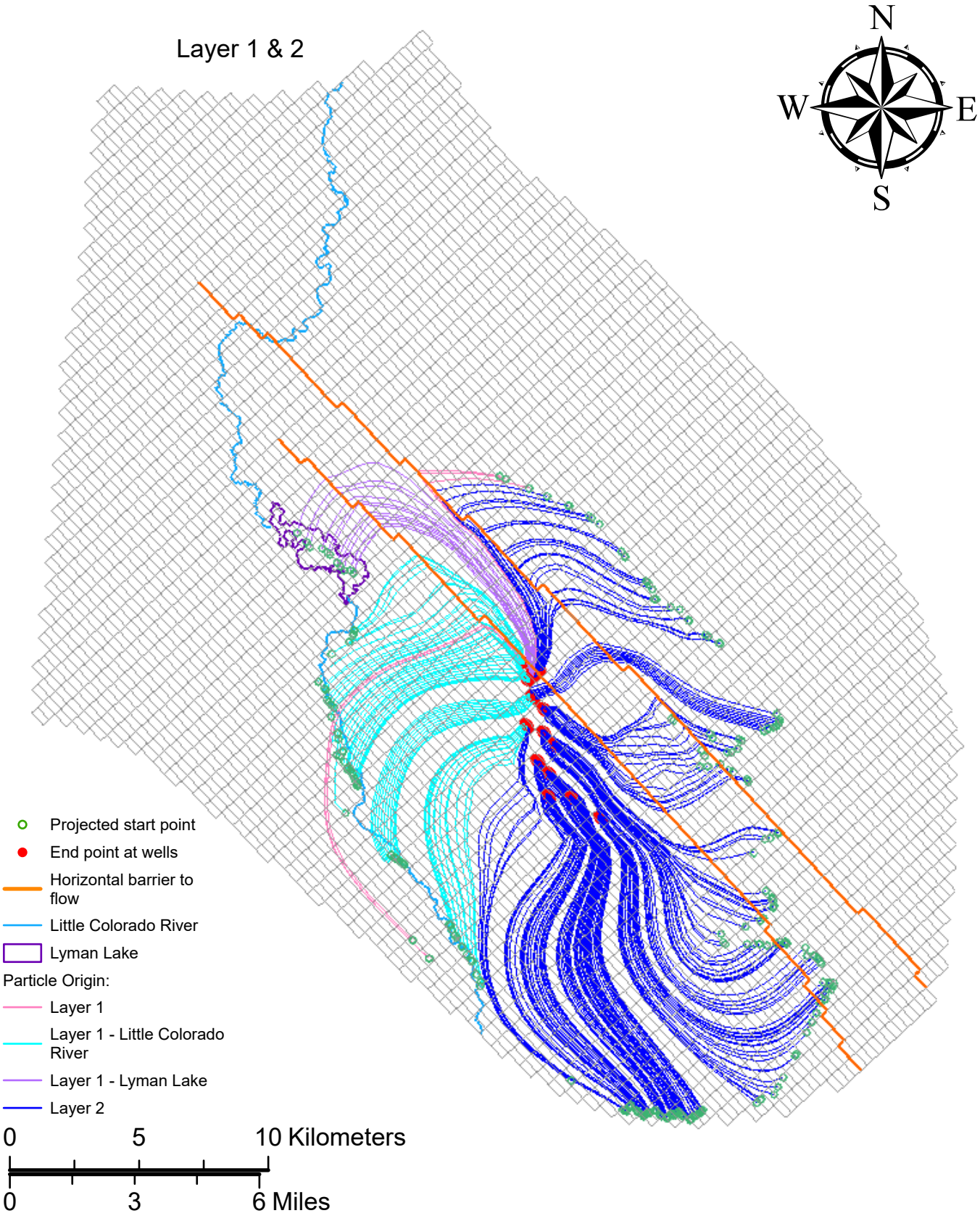

Figure 16: Backwards particle tracking for Particle Set A, generated at the calibrated model's active pumping wells and allowed to run until particles reached the end of their trajectories.

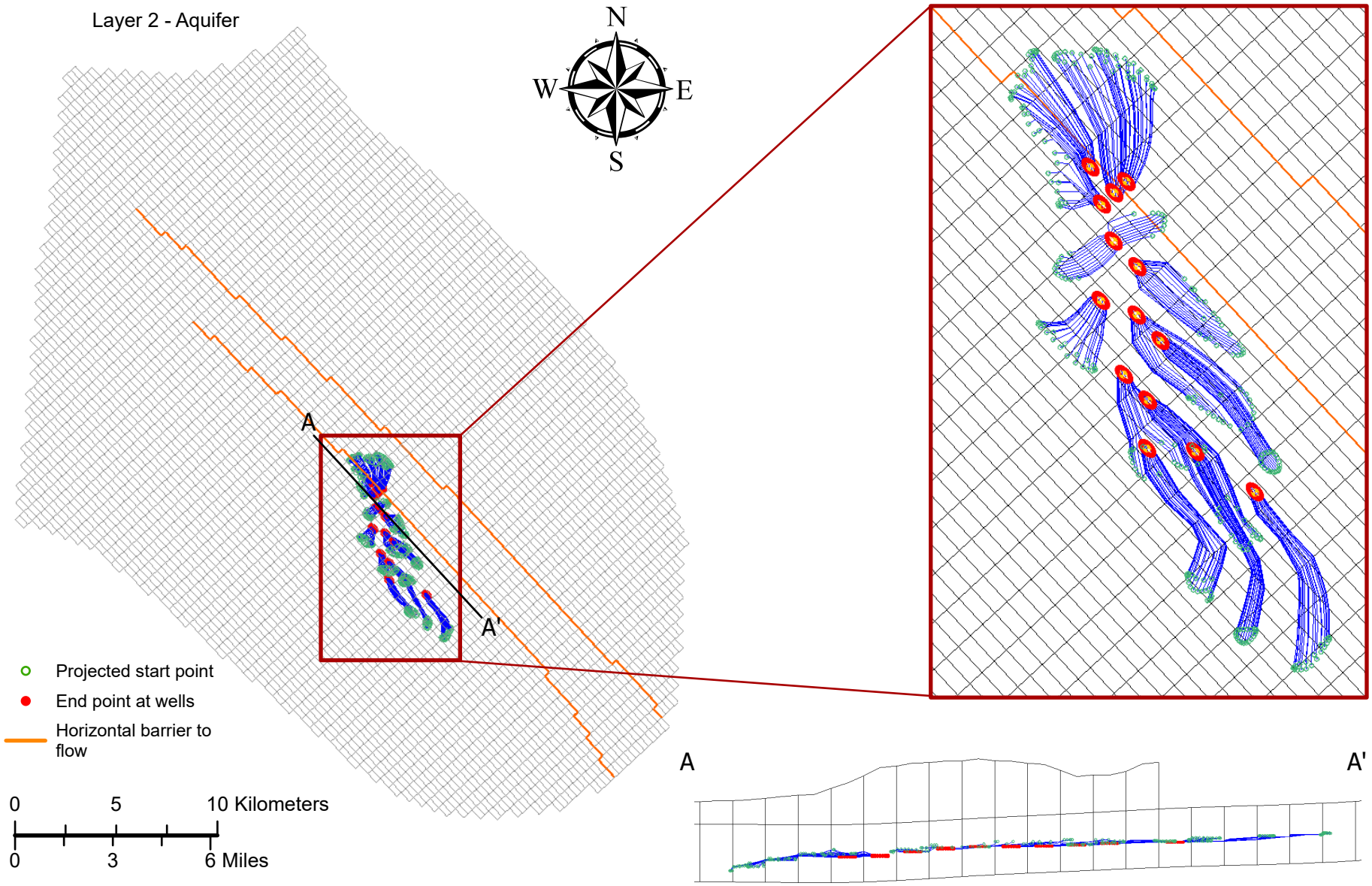

Figure 17: Backwards particle tracking for Particle Set A, generated at the calibrated model's active pumping wells with a run time of 13,514.25 days or 37 water years. This is the approximate length of time since pumping began in 1985 to 2023, present day. A-A' shows a cross-section view of the particles' travel path. All tracking particles are visible in the cross-sectional view, not just those that intersect the transect.

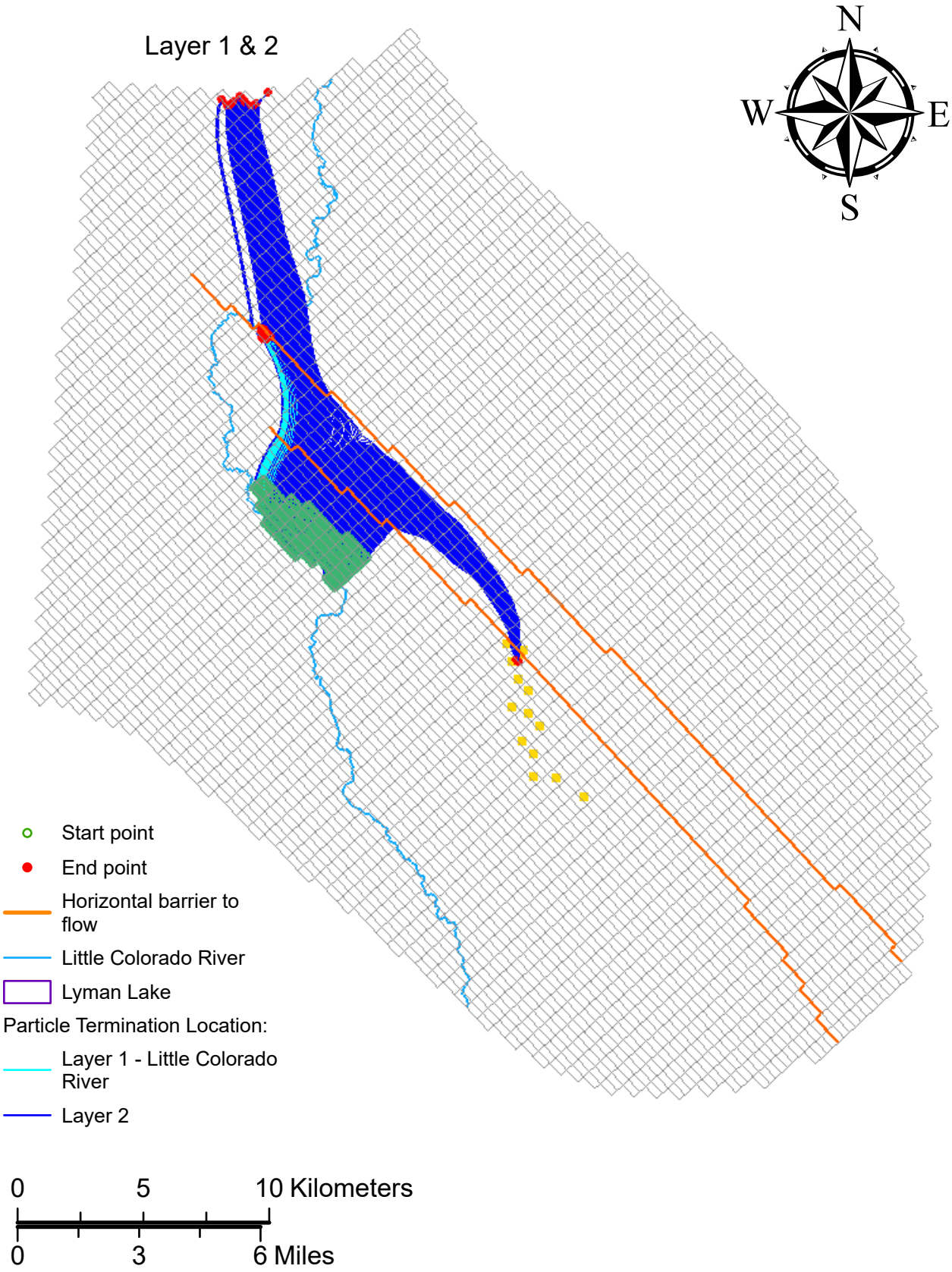

Figure 18: Forward particle tracking for Particle Set B, generated in the calibrated model at cells intersecting Lyman Lake and allowed to run until particles reached the end of their trajectories.

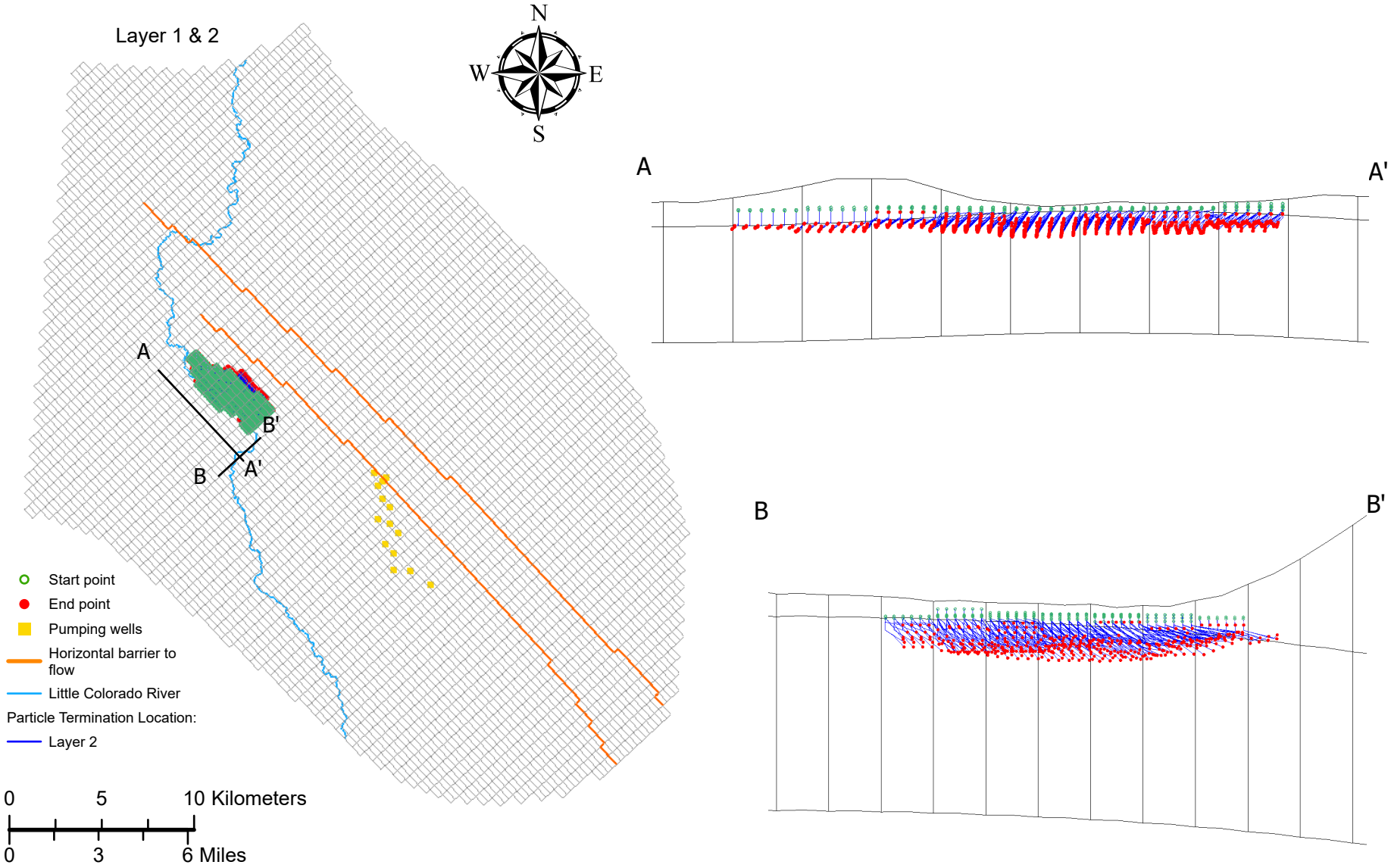

Figure 19: Forward particle tracking for Particle Set B, generated in the calibrated model at cells intersecting Lyman Lake, with a run time of 13,514.25 days or 37 water years. This is the approximate length of time since pumping began in 1985 to the present day (2023). Cross sections A—A' and B—B' show the particles' travel paths and predominant flow direction. All tracking particles are visible in the cross-sectional views, not just those that intersect the transects.

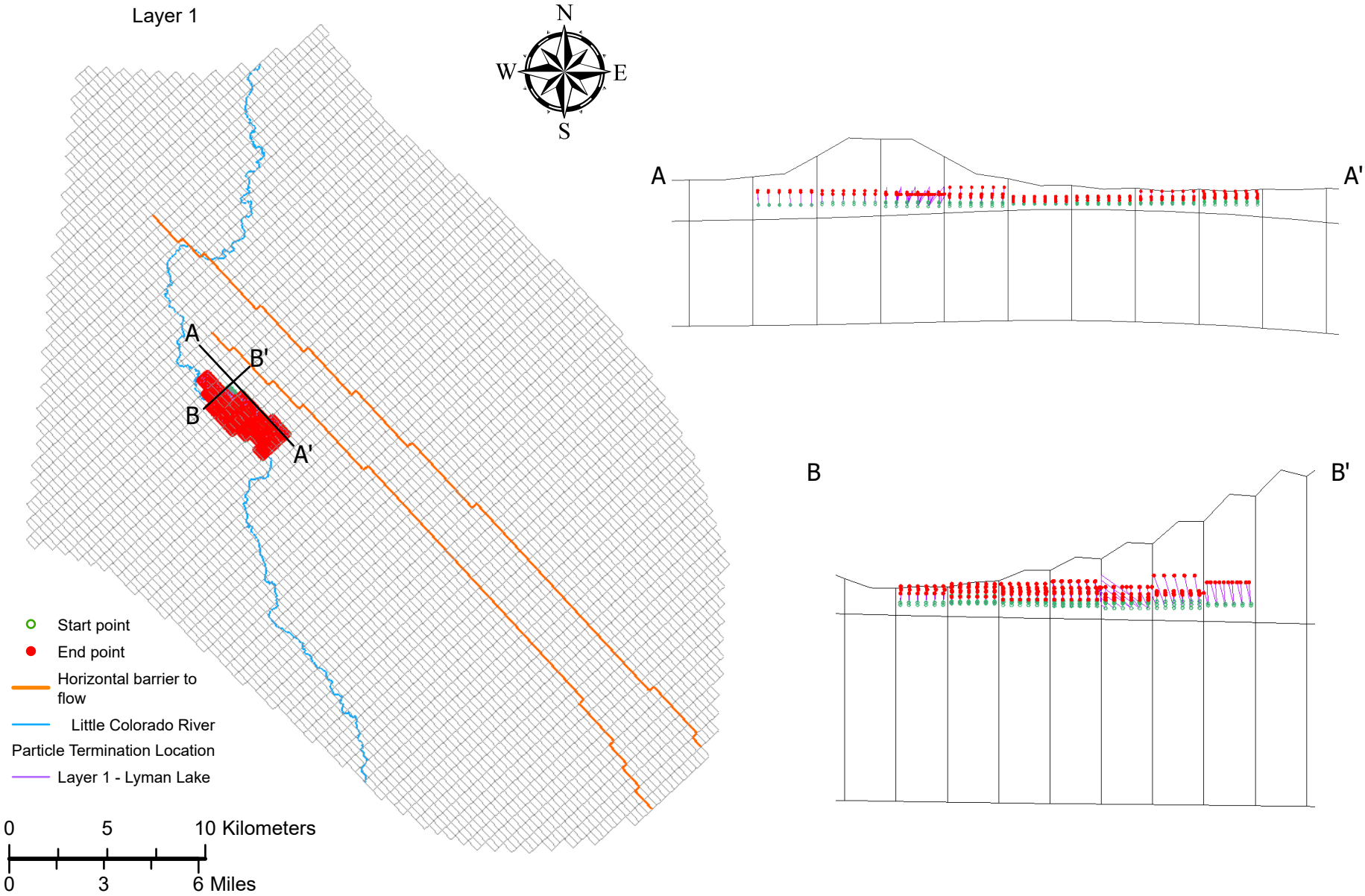

Figure 20: Forward particle tracking for Particle Set B, generated in the pre-pumping model. Particles were created at cells intersecting Lyman Lake and allowed to run until they reached the end of their trajectories. Cross sections A—A' and B—B' show the particles' travel paths and predominant flow direction. All tracking particles are visible in the cross-sectional views, not just those that intersect the transects.

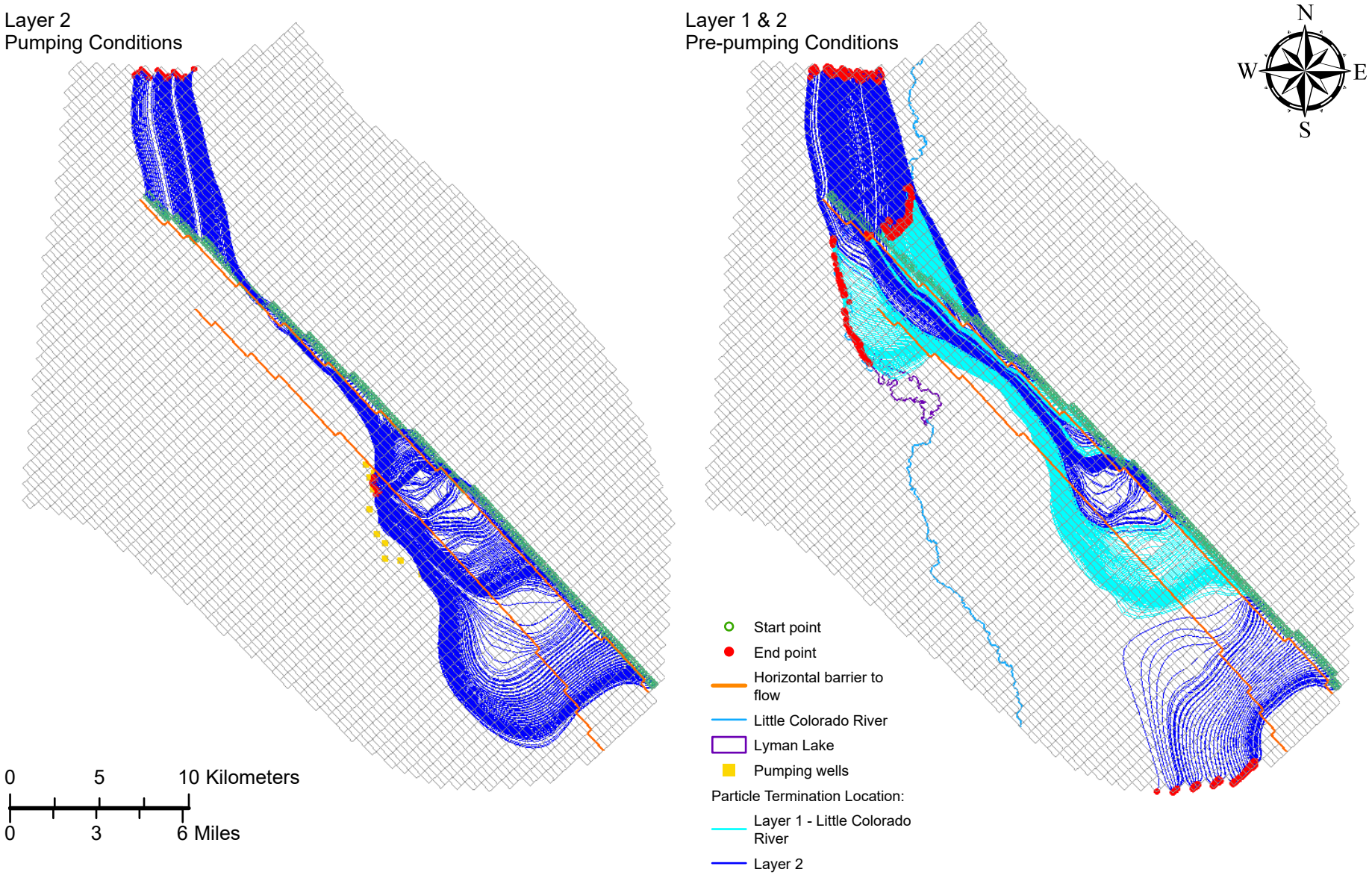

Figure 21: Forward particle tracking for Particle Set C, generated at cells running parallel to the Cedar Mesa anticline axis. For the simulation of pre-pumping conditions, turning off the pumping wells was the only altered parameter to the calibrated model.

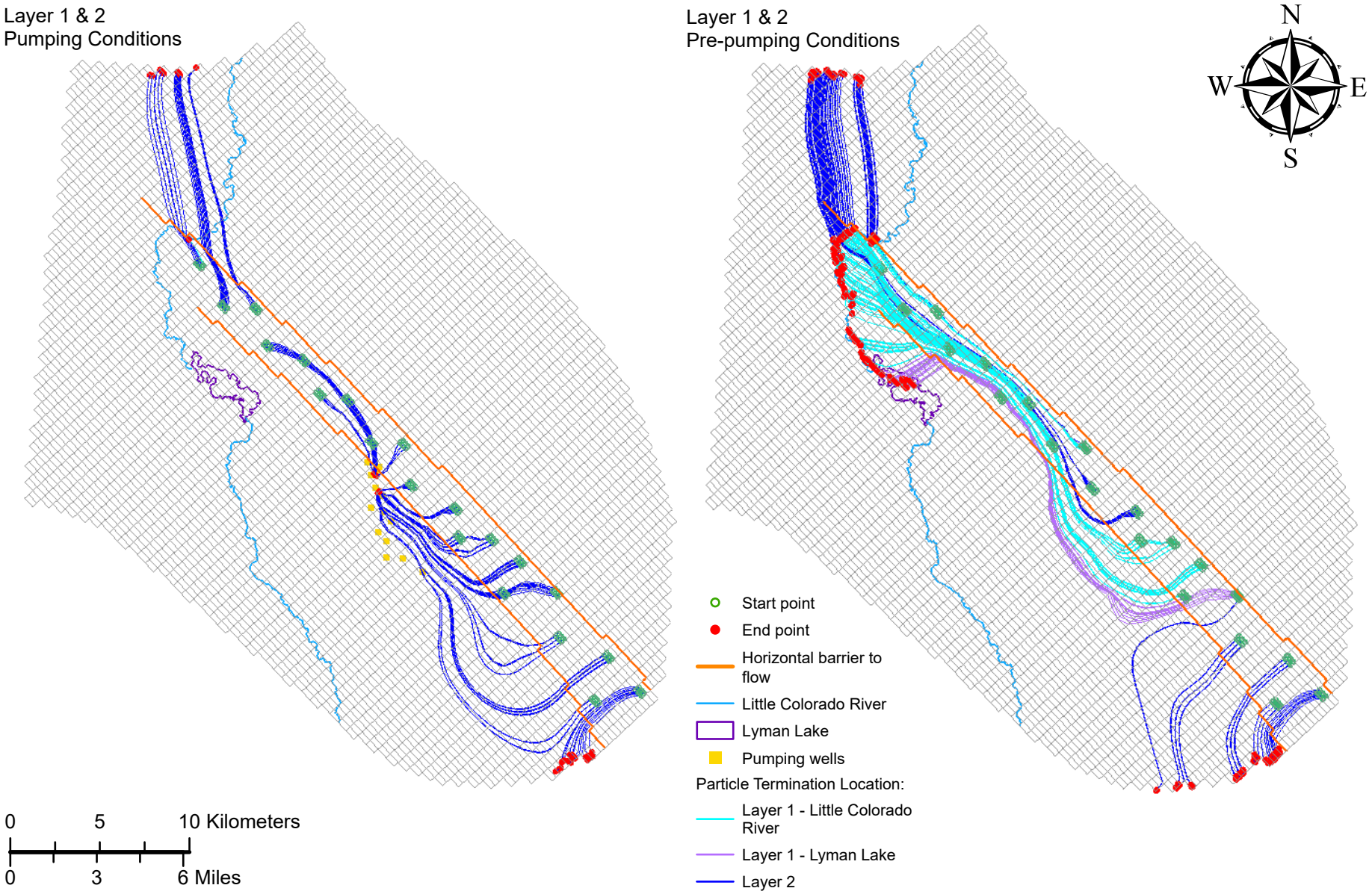

Figure 22: Forward particle tracking for Particle Set D, generated at cells located between the Cedar Mesa anticline axis and the Coyote Wash fault. For the simulation of pre-pumping conditions, turning off the pumping wells was the only altered parameter to the calibrated model.

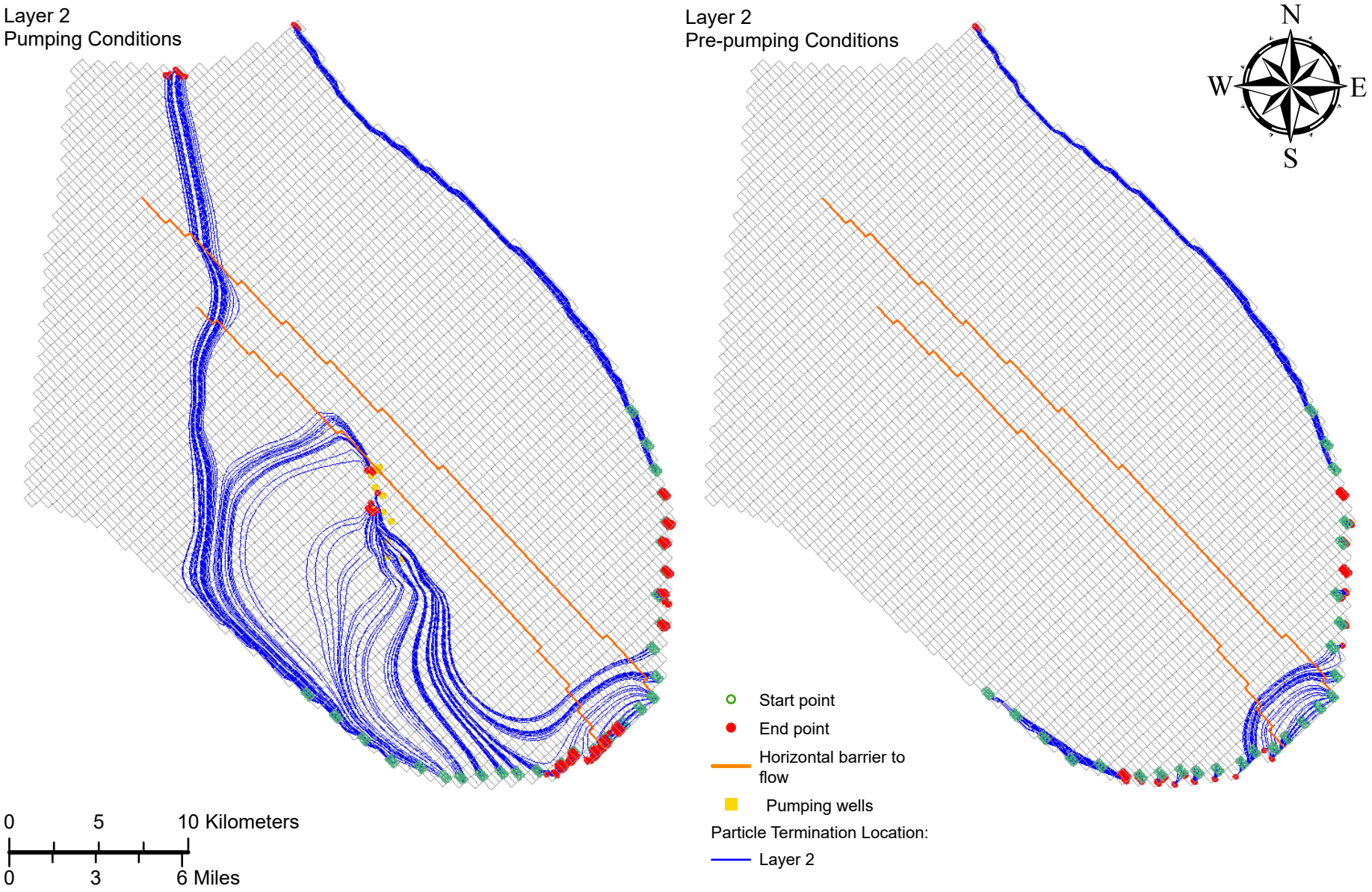

Figure 23: Forward particle tracking for Particle Set E, generated at cells located around the southern edge of the model. For the simulation of pre-pumping conditions, turning off the pumping wells was the only altered parameter to the calibrated model.

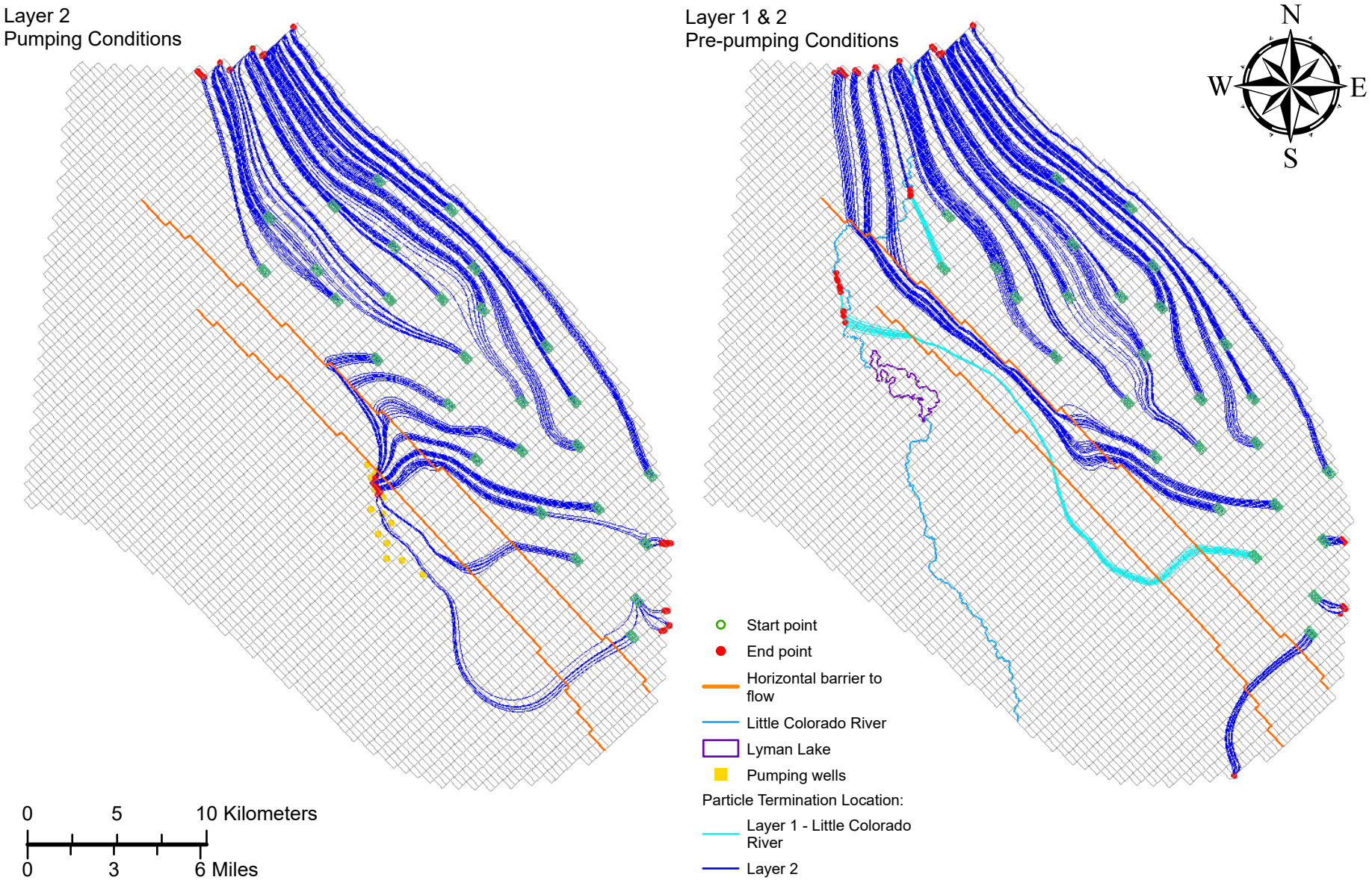

Figure 24: Forward particle tracking for Particle Set F, generated at cells located east of the Cedar Mesa anticline axis. For the simulation of pre-pumping conditions, turning off the pumping wells was the only altered parameter to the calibrated model.

Table 1. Average stream gage height and estimated river bottom sediments along the Little Colorado River as assigned to model nodes.[USGS, U.S. Geological Survey; N/A, not applicable]

Location on river	Gage number, source, info	River stage elevation (meters)	Estimated river bottom elevation[1] (meters)	Timespan of gage data (water years)
Little Colorado River at Wenima near Springerville, Arizona	9383595, USGS, retired	2118.9	2113.2	2009–2013
Little Colorado River above Lyman Lake, near St. Johns, Arizona	09384000, USGS, active	1832.6	1826.7	2008–2019
Point from DEM Below Lyman Lake, Little Colorado River and release from Lyman Lake, Arizona	N/A, this study, estimated based on aerial imagery	1808.3	1802.6	N/A
Little Colorado River, below Salado Springs, Arizona	09385700, USGS, active	1766.0	1758.1	2020, 2021
Point at north edge of study area, Little Colorado River, Arizona	N/A, this study, estimated based on aerial imagery	1727.4	1721.5	N/A
Little Colorado River above Zion Reservoir near St. Johns, Arizona	09386030, USGS, active	1695.0	1689.5	2008–2021

[1]Estimated river-bottom elevations are based on subtracting the estimated thickness of river-bed sediments (5.18 meters) from the datum. For estimated points where there was no stream gage data available, estimates were made from aerial imagery.

Table 2. Average pumping rate for active wells at Springerville Generating Station over their respective years of operation.

Well number	Flow rate[1] (cubic meters per day)	Years in operation
P-7/7A	−2975	1985–2018
P-8/8A	−3522	1990–2018
P-9/9A	−5276	1990–2018
P-10-10A	−4330	1985–2018
P-11-11A	−5010	1985–2018
P-12-12A	−5090	1990–2018
P-14-14A	−3436	1985–2018
P-15	−5249	2004–2018
P-16	−3254	2006–2018
P-17	−5009	2006–2018
P-18	−6211	2009–2018
P-19	−5311	2009–2018
P-20	−3476	2009–2018
P-21	−5776	2017–2018

[1]Negative sign on the flow rate is due to MODFLOW settings and reflects that these are extraction wells.

Table 3. Borehole data with horizon contact elevations in meters (m).

Borehole name	Elevation above sea level					Bottom elevation, Horizon 1	Elevation of maximum drilled depth (m)	Comment[1]
	Horizon 6	Horizon 5	Horizon 4	Horizon 3	Horizon 2			
85W	1788.0	1752.6	1664.2	1597.8	1531.3	1491.0	1531.3	Idealized contact for Horizon 1.
533974 - Grover's	1770.1	1742.7	1689.4	1620.8	1561.3	1521.0	1556.8	Idealized contact for Horizon 1.
220655 - Salt River		1810.1	1761.3	1689.7	1618.0	1578.0	1387.6	Idealized contact for Horizon 1.
CCR-1U	2118.3	2081.7	1997.6	1922.6	1856.2	1816.0	1856.2	Idealized contact for Horizon 1.
CCR-2D	2082.8	2046.2	1967.2	1879.8	1799.3	1759.0	1778.0	Gamma-ray and induction logs were used to identify the top of the contacts for Moenkopi Formation and lower units.
CCR-3D	2093.3	2090.2	1967.4	1878.4	1799.8	1759.0	1799.8	Some uncertainty in the well log for the estimated depths of contacts. Idealized contact for Horizon 1.
E-4	2048.0	2029.7	1918.4	1804.1	1715.8	1675.0	1682.2	Idealized contact for Horizon 1.
E-8	1990.5	1874.7	1697.9	1591.2	1518.1	1478.0	1518.1	Idealized contact for Horizon 1.
M-9		2010.1	1921.7	1842.5	1766.3	1726.0	1766.3	Idealized contact for Horizon 1.
P-4	2063.5	2045.3	1980.3	1892.6	1807.5	1767.0	1773.1	Idealized contact for Horizon 1.
P-6	2104.5	2071.0	2010.3	1914.9	1830.2	1790.0	1799.7	Idealized contact for Horizon 1.
P-9A	1999.5	1978.2	1853.2	1740.4	1655.1	1615.0	1655.1	Idealized contact for Horizon 1.

Borehole name	Elevation above sea level					Bottom elevation, Horizon 1	Elevation of maximum drilled depth (m)	Comment[1]
	Horizon 6	Horizon 5	Horizon 4	Horizon 3	Horizon 2			
P-10A	2019.0	1970.3	1817.9	1708.1	1628.9	1588.0	1628.9	Idealized contact for Horizon 1.
P-11	2012.1	1990.7	1787.1	1681.1	1593.0	1552.0	1577.7	Idealized contact for Horizon 1.
P-14A	1994.7	1894.1	1753.9	1644.2	1568.0	1528.0	1568.0	Idealized contact for Horizon 1.
P-16	2001.4	1961.8	1804.8	1696.6	1623.5	1583.0	1599.1	Idealized contact for Horizon 1.
P-17	2007.7	1934.5	1776.0	1672.4	1587.1	1547.0	1587.1	Idealized contact for Horizon 1.
P-18	2005.4	1981.0	1767.7	1670.1	1581.8	1541.0	1581.8	Idealized contact for Horizon 1.
P-20	2012.6	1988.2	1822.1	1713.9	1631.6	1591.0	1631.6	Idealized contact for Horizon 1.
504188 - Merrill	2137.7	2136.8	2093.5	1991.4	1893.9	1853.0	1893.9	Idealized contact for Horizon 1.
527306 - Salt River	1916.4	1895.1	1828.0	1724.4	1648.2	1608.0	1648.2	Idealized contact for Horizon 1.

[1]Comments indicate any modifications that were made to the original record for the purpose of generating solids that reflect the best understanding of real-world conditions.

Table 4. Computational errors, calculated in MODFLOW, between the observed heads and calculated heads.

Property	Value (meters)
Mean residual (head)	0.18
Mean absolute residual (head)	1.17
Root mean squared residual (head)	1.95

Table 5. All parameter values calculated and refined during model calibration, excluding Layer 2 pilot-point hydraulic conductivity values (Tables 6, 7).

[m, meter; m/d, meter per day; $(m^2/d)/m$, square meter per day per meter; $(m^2/d)/m^2$, square meter per day per square meter]

Location	Value
Hydraulic characteristic	
Coyote Wash fault	1.0
Cedar Mesa anticline	0.00010
General head boundary stage	
North boundary	1673 m
South boundary from the Coyote Wash fault westward	1862 m
South boundary from the Cedar Mesa anticline eastward	1960 m
Hydraulic conductivity	
Zone 1	0.0969 m/d
Zone 2	0.00325 m/d
Recharge	
Zone 1	0.802×10^{-8} m/d
Zone 2	0.659×10^{-4} m/d
Zone 3	0.135×10^{-3} m/d
River conductance	
Upstream of Lyman Lake	0.104 $(m^2/d)/m$
Downstream of Lyman Lake	0.0599 $(m^2/d)/m$
General head boundary conductance	
Lyman Lake	0.900×10^{-4} $(m^2/d)/m^2$

Table 6. Parameter estimation of hydraulic conductivity, in meters per day, for pilot points in Zone 3, located outside the model fault zones in Layer 2.

Zone 3 pilot point identifier	Hydraulic conductivity
1	0.0210
2	0.254
3	0.776
4	0.124
5	2.00
6	1.02
7	1.90
8	0.107
9	1.60
10	0.0131
11	0.909
12	0.541
13	0.0110
14	1.22
15	0.0240
16	1.02
17	4.70
18	0.0178
19	4.67
20	0.0107
21	1.18
22	3.95
23	0.0200
24	0.0103
25	12.0
26	0.0530
27	0.0787
28	0.0111
29	2.42

Zone 3 pilot point identifier	Hydraulic conductivity
30	0.0465
31	0.0110
32	3.30
33	0.453
34	0.0949
35	10.8
36	0.152
37	0.997
38	1.70
39	0.818
40	6.44
41	0.334

Table 7. Parameter estimation of hydraulic conductivity, in meters per day, for pilot points in Zone 4, located within the model fault zones in Layer 2.

Zone 4 pilot point identifier	Hydraulic conductivity
1	40.0
2	40.0
3	40.0
4	40.0
5	15.4
6	40.0
7	38.8
8	8.68
9	23.2
10	3.06
11	22.1
12	33.4
13	37.6
14	0.00117
15	0.311
16	0.0236
16	0.0236
17	33.0
18	40.0
19	1.09
20	0.000830
21	0.00805
22	2.04
23	0.00712
24	0.207
25	0.0999
26	0.000296
27	0.0942
28	0.00115

Zone 4 pilot point identifier	Hydraulic conductivity
29	0.595
30	0.0153
31	0.0840
32	23.3
33	40.0
34	0.867
35	31.9
36	8.91
37	0.0967
38	26.4
39	2.93
40	5.84
41	33.1
42	0.691
43	0.785
44	40.0
45	1.72
46	1.23
47	40.0
48	0.589
49	0.880
50	0.0237

Table 8. Calibrated recharge values in meters per day (m/d).

Recharge zone	Starting value[1] (m/d)	Model-calibrated value[2] (m/d)
Zone 1	0.300×10^{-3}	0.802×10^{-8}
Zone 2	0.359×10^{-3}	0.659×10^{-4}
Zone 3	0.407×10^{-3}	0.135×10^{-3}

[1]Calculated using PRISM precipitation values and Normalized Difference Vegetation Index evapotranspiration values for the study area.

[2]Determined using MODFLOW's parameter estimation (PEST).